Explaining the multiple energy thresholds for damage mechanisms activation in laminate composites under cyclic loadings

Ferreira Motta, Roberto; Alderliesten, René; Zarouchas, Dimitrios; Yutaka Shiino, Marcos; Odila Hilario Cioffi, Maria; Jacobus Cornelis Voorwald, Herman

Important note
To cite this publication, please use the final published version (if applicable).
Please check the document version above.

Explaining the multiple energy thresholds for damage mechanisms activation in laminate composites under cyclic loadings

Roberto Ferreira Motta Jr. [a], René Alderliesten [b], Dimitrios Zarouchas [b], Marcos Yutaka Shiino [c], Maria Odila Hilario Cioffi [a], Herman Jacobus Cornelis Voorwald [a]

[a] *São Paulo State University (Unesp) - Materials and Technology Department - Fatigue and Aeronautic Materials Research Group, Guaratinguetá - SP, Brazil*
[b] *Aerospace structures and Materials Department, Faculty of Aerospace Engineering, Delft University of Technology, P.O. Box 5058, 2600 GB Delft, the Netherlands*
[c] *São Paulo State University (Unesp) – Institute of Science and Technology, São José dos Campos - SP, Brazil*

ARTICLE INFO

ABSTRACT

After half a century of developing fatigue delamination prediction models, where accuracy seems more important than physical understanding, this research aims to merge both aspects. To that aim, strain energy release (SER) within the fatigue load cycle was studied using acoustic emission. The correlation between the measured strain energy release and the acoustic emission energy was formulated through a conversion factor to convert one into the other. The strain energy release distribution within the loading cycle indicated that different damage mechanisms are activated in different increments of the load cycle associated with different energy thresholds. The presence of multiple energy thresholds indicated that the application of different loading cycles results in distinct resistances to damage propagation (*dU/dA*) depending on which energy threshold is crossed.

1. Introduction

The quest of the industry transportation sectors for achieving structural efficiency through weight reduction has increased the efforts to employ fiber-reinforced polymers (FRP) in primary structures. The structural FRP composites are usually laminates with no reinforcement fibers in the thickness direction, which reduces the interlaminar strength of the material leading to delamination susceptibility [1]. Delamination is the main barrier to the broader use of FRP composites in primary structures and can be roughly defined as the separation of two adjacent laminae by a planar crack that splits the fiber plies due to out of plane (mode I) and shear (mode II) stresses.

Fatigue is one of the main reasons for delamination growth. This propagation process degrades the structure and can lead to a catastrophic failure if the damage reaches a critical size. Therefore, a comprehensive fatigue delamination growth (FDG) characterization is required to enable structural damage tolerant design and to increase the reliability of composite structures [2–7]. Consequently, an extensive number of models to predict FDG has been proposed by numerous researchers [8–23]. However, their development frequently relied on successive attempts to obtain an equation capable of describing the experimental data trend. In other words, these models were developed phenomenologically, with little explanations on their physical meaning

[24–27].

In general, FDG prediction models are based on a Paris-type curve that follows a power-law form (Eq. (1)) [24,26], i.e.,

$$\frac{da}{dN} = Cf(G)^n \tag{1}$$

in which *da/dN* is the crack growth rate, *G* is the strain energy release rate (*SERR*), and *C* and *n* are empirical parameters determined by curve fitting.

The Paris relation is based on the similitude principle, in which a scaling law is fitted to parameters describing similarity in conditions (here the *SERR*) and the observed consequences (here the *da/dN*). This principle allows to relate laboratory tests to full-scale structures but does not necessarily formulate a physical causal relationship to explain this relation [28]. Additionally, the variation of some testing conditions capable of changing the *da/dN* behavior, such as the *R*-ratio [10–15], the presence of mixed-mode loading conditions [19–22], and the fiber bridging content [29–31], led to the creation of a substantial number of models trying to account for these factors [32]. Consequently, there is no consensus on which model or similitude parameter should describe crack propagation in laminates judging the many different options proposed so far [28,33,34]. For this reason, the delamination growth due to fatigue must be thoroughly investigated to allow the formulation of physical explanations for the FDG process, aiming to establish a

Nomenclature

A	*delamination area (mm^2, m^2)*
a	*delamination length (mm)*
d	*displacement (mm)*
E	*acoustic energy (aJ)*
G	*strain energy release rate (mJ/mm^2)*
N	*number of cycles*
P	*force (N)*
R	*displacement ratio*
U	*strain energy (mJ)*

Subscripts

c	*critical*
cyc	*cyclic*
max	*maximum*
min	*minimum*
n	*number of cycles*
th	*threshold*
tot	*total*

suitable and general prediction model for composites.

1.1. Acoustic emission (AE) technique potential to investigate damage propagation within loading cycles

The *SERR* or *G* used to describe similitude is fundamentally an energy parameter. Therefore, the crack growth process should agree with the energy balance concept first proposed by Griffith, which states that the amount of energy released (G) due to a stable propagation of a crack should be equal to the amount of energy required to create new fracture surfaces (G_c) [35]. In this approach, *G* corresponds to the driving force, while G_c is defined as the material resistance to crack propagation under fixed-grip and quasi-static loading conditions. As a consequence of this formulation, *G* is treated as the driving force rather than resistance in most models developed so far to predict FDG [24]. However, the physical definition of *G*, i.e., the strain energy released (SER) per area due to crack propagation, corresponds to the definition of resistance, allowing the interpretation of *G* as the consumption side of the Griffith's energy balance equation. In other words, *G* can be defined as the material resistance to crack propagation.

In the present work, the strategy adopted to study the laminate resistance to FDG was to investigate the SER within the loading cycles. Considered it, the Griffith's energy balance, the strain energy released within a single loading cycle should be proportional to the damage propagated within this cycle. However, quantifying damage propagation within a single loading cycle is challenging, which explains why current FDG models generally consider an average damage propagation over a sequence of cycles [36–41], while a few studies try to investigate the propagation process within these cycles [32,42–44]. This lack of accuracy to quantify damage formation hinders the crack propagation discontinuity and inhibits detecting the microscopic and stochastic nature of the underlying damage mechanisms [24,32,42], suppressing physical understanding. In this contest, researchers have appealed to non-destructive evaluation (NDE) techniques in order to collect more information about damage propagation in composites [45–47].

Recently, the AE technique has been one of the most used NDE techniques in structural health monitoring due to its ability to provide In-Situ information during testing [48]. Every time a single damage event occurs inside a specimen or a structure (e.g., crack nucleation and propagation in the matrix, cohesive or adhesive failure of fiber/matrix interface, and rupture of single filaments or bundles of fibers), there is a spontaneous release of energy due to rapid internal displacements,

originating ultrasonic waves [49]. The AE technique can detect these signals using piezoelectric sensors attached to the surface of the material, which means that information from damage formation during the entire load history of the structure can be obtained. However, it is essential to know the AE parameters (e.g., rise time, energy, counts, duration, peak amplitude, and peak frequency) used to describe each ultrasonic signal and understand how the test conditions affect them to assess the experimental data properly, allowing not only damage detection but also damage identification [50,51], damage location [52,53], and the elimination of eventual noise recorded along with the data [54].

Moreover, the AE technique is capable of continuously monitoring the material under loading, making this technique suitable to investigate damage propagation within loading cycles in fatigue, as studied in the works of Pascoe *et al.* [32], Dzenis *et al.* [43], and a previous work developed by the authors [42]. Pascoe *et al.* [32] defined the concept of energy threshold (G_{th}), i.e., the minimum amount of energy required to damage propagation onset within a single loading cycle, and observed that the damage propagation might occur during both loading and unloading. Dzenis *et al.* [43] observed a concentration of acoustic signals related to damage propagation at high stresses even during the unloading section of the cycles. Xiang *et al.* [44] developed a subcycle delamination growth model assuming there is no delamination growth during the unloading and below a threshold load level during the loading. In [42], the authors observed acoustic signals with different features in different regions of the cycles, which indicates the activation of distinct damage mechanisms in different segments of the cycles. This observation led to the key question for the development of the present work: do different damage mechanisms require distinct energy levels for their activation?

Several models to predict FDG proposed in literature use a critical or threshold energy release rate (G_c or G_{th}) to quantify a minimum amount of energy required to damage onset in fatigue [12,14,15,18,23,55]. This research demonstrates that the activation of distinct damage mechanisms in different stages of the load cycles, as suggested in [42], is associated with multiple energy thresholds rather than the single energy threshold to damage onset considered in the literature. In addition, the actual research does not aim to develop a new model but to explain the concept of multiple energy thresholds, which is essential for developing more accurate prediction models in future works.

2. Materials and methods

The methodology developed to exhibit the presence of multiple energy thresholds for damage onset within the loading cycles is straightforward and is based on the SER behavior. The strain energy stored in the material is released due to damage propagation. Hence, it is reasonable to assume that every time a new energy threshold is crossed within the loading cycle, more strain energy is released due to the activation of new damage mechanisms. Thus, the SER within the loading cycles must be quantified. For this purpose, the present work developed a methodology to determine the strain energy released within the loading cycles using acoustic emissions through a conversion factor.

2.1. Specimen preparation and specifications

Mode I quasi-static and fatigue delamination propagation was investigated using double cantilever beam (DCB) specimens obtained from a glass fiber reinforced polymer (GFRP) laminate. The laminate was manufactured using the resin transfer molding (RTM) technique, and twelve biaxial stitched silane treated glass fiber layers stacked up in a quasi-isotropic [(-45°/45°)/(90°/0°)]$_{3S}$ lay-up were placed in the cavity of a metallic mold. At this stage, a polytetrafluoroethylene film with 13 μm thickness was inserted between the 0°/0° mid-plane interface to produce an artificial pre-crack of 30 mm length measured from the loading line. Once the mold was completely sealed, the

monocomponent HexFlow RTM6 epoxy resin system (supplied by Hexcel) was injected into the mold cavity with a pressure of 2 bar (0.20 MPa) under a constant temperature of 100 °C, and a vacuum pressure of 0.5 bar (50 kPa). After the complete impregnation of the laminate, the resin was cured at 180 °C for 120 min.

The DCB specimen dimensions complied to ASTM D5528-13 [56] with a width of 24.93 mm ($\pm$0.17), length of 150 mm, and thickness of 3.33 mm ($\pm$0.06), resulting in a fiber volume fraction of 65.17 % ($\pm$1.57) determined by acid digestion following ASTM D3171-15 [57]. Aluminum blocks were bonded at both sides of one end of the specimen for load application, as shown in Fig. 1. One side of the specimen was coated with a thin layer of type-writer correction fluid (white color) to enable better visualization of the crack tip, and a scale in millimeters was added for crack length measurements during the tests (see detail A in Fig. 1). In addition, the combination of the epoxy resin and the glass fibers produced a translucid laminate that allowed following the crack tip at the top of the specimen (see detail B in Fig. 1). Then, the crack length measurements at the edges could be verified.

2.2. Test program and experimental set up

Aiming to investigate the correlation between acoustic and strain energies, a test program was developed considering different load conditions, as presented in Table 1.

Table 1. Test parameters and specimens' identification.

The tests listed in Table 1 enable to evaluate the influence of the applied loading condition (quasi-static or fatigue with different *R*-ratios), the amount of fiber bridging, and the crack growth rate on the correlation between acoustic and strain energies. The amount of fiber bridging was varied by testing the specimen FT1 three times in fatigue, increasing d_{max} until a critical value was reached in every test, as described in the ESIS-TC4 test protocol [58]. The fiber bridging is minimal in the first fatigue test sequence (artificial pre-crack) and increases during the subsequent test sequences due to the bridging length increase. The loading frequency was reduced at higher d_{max} by maintaining a constant displacement rate (30 mm/s), because the test machine could not maintain the frequency at 3.82 Hz at larger displacements. The crack growth rate range was changed by reducing d_{max} in the tests of specimens FT4, FT5, and FT6 by 10, 15, and 20 %, respectively.

Prior to all tests, the artificial pre-crack was opened with a constant displacement rate of 1 mm/min until reaching a pre-crack length of 34 mm. The specimens were submitted to at least 4×10^5 loading cycles using an MTS 100 kN servo-hydraulic fatigue machine equipped with a 1 kN load cell. The crack length was monitored with a camera (Optomotive high-resolution digital camera, Mechatronics ltd) focused at the painted side of the specimen with the acquisition rate of one photo every-three seconds in quasi-static tests and every 100 cycles in fatigue

tests. The fatigue machine, the image acquisition system, and the AE system were synchronized to allow correlations between load, displacement, AE signals, and the number of cycles.

2.2.1. AE set up: Threshold definition and noise filtering

The 8-channel AMSY-6 Vallen AE system with four parametric inputs was used to monitor crack propagation during the tests. A wide-band piezoelectric sensor (VS900-M) with an operating frequency ranging between 100 and 900 kHz was attached to the specimen free end using a clamp, and grease was used as coupling fluid as illustrated in previous work, see references [32,42]. The piezoelectric sensor was connected to an external pre-amplifier with a band-pass filter of 20–1200 kHz. The sampling rate used in the tests was 2 MHz, and the pencil lead break procedure was used to assure reproducibility of the sensor response at the specimen's surface [59]. The amplitude threshold for the recorded signals was set at 55 dB, which is suitable for fatigue tests but might be considered high for quasi-static loading conditions. However, this limit was set to both quasi-static and fatigue tests in order to compare the AE results since a different AE threshold would affect almost all the parameters of the acoustic waves detected during the test. This 55 dB AE threshold was established based on the literature [32,43,60] and a previous work conducted by the authors [42], considering that a lower amplitude threshold in fatigue would increase the noise recorded by the AE system.

It is impossible to define a threshold that ensures the complete elimination of the noise without eliminating a few acoustic emissions related to damage. There is an amplitude range in which both noise and low-energy damage signals are recorded, inhibiting the total elimination of the noise using the AE parameters because they mostly overlap each other, as observed by Dzenis *et al.* in [43]. Hence, the present research uses only the energy of the signals in the analysis to minimize the effect of undesirable detection or elimination of low-energy signals.

In general, it is expected that the noise has a low intensity, allowing them to be filtered by the threshold. However, the mode I fatigue tests using double cantilever beam (DCB) specimens generates noise with relatively high amplitudes due to the friction of the fracture surfaces. The friction is restricted to regions of the cycle close to the minimum displacement (d_{min}), where the damage formation rate tends to be relatively low or absent due to the low strain energy state of the specimen, allowing the elimination of the noise without eliminating a relevant amount of signals related to damage formation. Additionally, previous works observed that the noise detection due to friction was substantially higher at the unloading than at the loading section of the cycles [42,43]. Thus, the hits (hit is an AE signal recorded on one channel) detected at the unloading region below 65 % of d_{max} were disregarded and interpreted as friction noise. The displacement threshold of 65 % was established based on analyses of the acoustic signals' distribution within the loading cycles (see the example in Fig. 2)
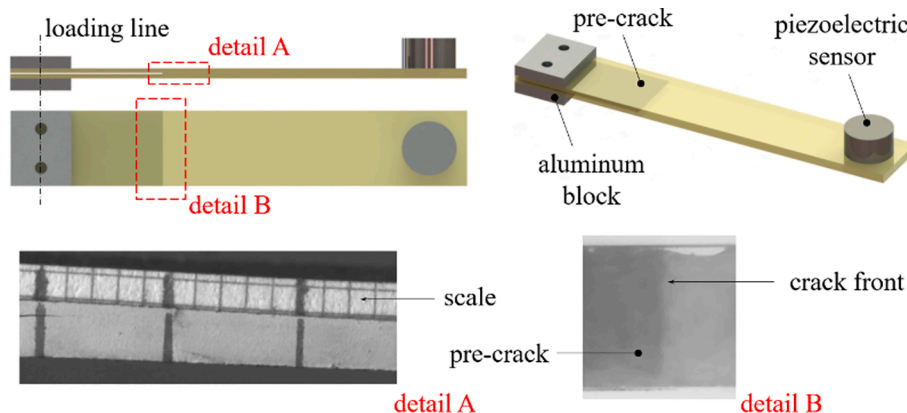

Fig. 1. Specimen configuration.

Table 1
Test parameters and specimens' identification.

| Specimen	Loading condition	Pre-crack length (mm)	Displacemen rate	Frequency (Hz)	d_{max} (mm)	d_{min} (mm)	R
QS1	Quasi-static	34.0	1.0 mm/min	–	–	–	–
QS2	Quasi-static	34.0	1.0 mm/min	–	–	–	–
QS3	Quasi-static	34.0	1.0 mm/min	–	–	–	–
FT1	Fatigue	34.0	30.0 mm/s	3.82	4.36	0.436	0.1
*FT1-2	Fatigue	48.4	30.0 mm/s	2.38	7.00	0.700	0.1
*FT1-3	Fatigue	60.8	30.0 mm/s	1.72	9.70	0.970	0.1
FT2	Fatigue	34.0	30.0 mm/s	3.82	4.36	0.436	0.1
FT3	Fatigue	34.0	30.0 mm/s	3.82	4.36	0.436	0.1
FT4	Fatigue	34.0	26.9 mm/s	3.82	3.92	0.392	0.1
FT5	Fatigue	34.0	25.5 mm/s	3.82	3.71	0.371	0.1
FT6	Fatigue	34.0	24.0 mm/s	3.82	3.49	0.349	0.1
FT7	Fatigue	34.0	16.7 mm/s	3.82	4.36	2.180	0.5
FT8	Fatigue	34.0	16.7 mm/s	3.82	4.36	2.180	0.5
FT9	Fatigue	34.0	16.7 mm/s	3.82	4.36	2.180	0.5
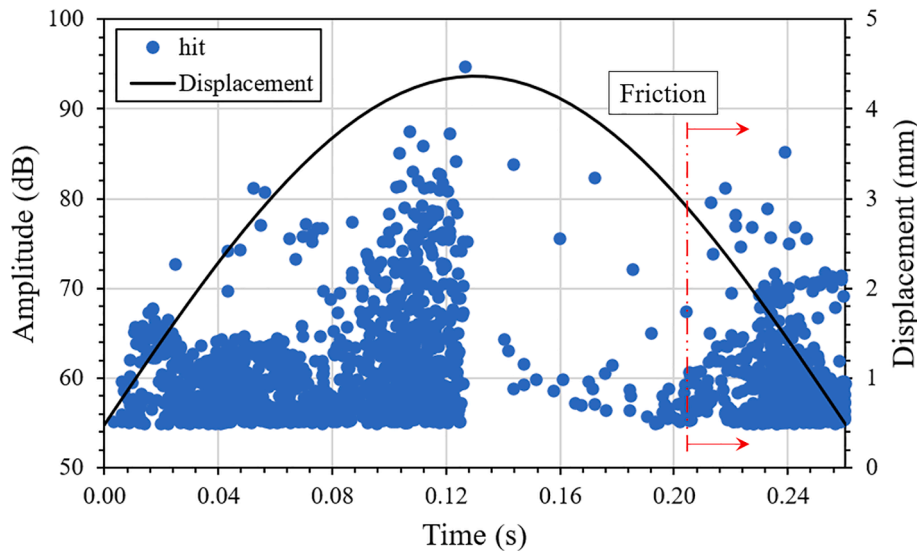
Fig. 2. Distribution of the hits detected within the loading cycles until a crack length of 2 mm measured from the pre-crack: specimen FT3 (R = 0.1).

and the works of Dzenis *et al.* [43] and Motta *et al.* [42].

2.3. Procedure for correlating strain energy release (dU) and acoustic energy release (dE)

When a crack propagates within the specimen, strain energy is released from the surrounding material, and an equal amount of energy should be dissipated within the system to keep the theoretical energy balance. The development of damage events dissipates acoustic energy within the system. For this reason, the acoustic energy (defined as the area beneath the squared waveform within the waveform's duration [61]) was chosen to be correlated with the strain energy released from the surrounding material amongst all the AE parameters, so two energy quantities could be compared. In this work, "acoustic energy dissipation" will be referred to as "acoustic energy release" to ease the discussions. However, the term "dissipation" is more suitable for acoustic energy.

Sections 2.3.1 and 2.3.2 describe the procedures developed to correlate both energy releases in quasi-static and fatigue delamination propagation to find a conversion factor between both energies. In the following analysis, the internal elastic strain energy stored in the specimens will be referred to as *U*, which corresponds to the definition of *G* as physics-based characterization of resistance (Eq. (2)), i.e., the release of strain energy (*dU*) per crack area (*dA*).

$$G = -\frac{dU}{dA} \tag{2}$$

According to the physical definition of *G*, G_{th} would represent the strain energy release **rate** at the instant prior to damage onset. However, *G* is a consequence of damage propagation and must be attributed to a certain amount of crack growth. In this research, U_{th} corresponds to the total strain energy stored in the specimen at the instant prior to damage onset. Additionally, previous works showed that U_{tot} correlates with resistance [28]. Thus, the minimum amount of energy required to damage onset within a single loading cycle is referred to as U_{th} instead of G_{th} in this work.

2.3.1. Quasi-static delamination propagation

The correlation is possible based on the assumption that both energies (acoustic and strain) are released due to damage propagation. Fig. 2 illustrates the concept of correlating the released energies between subsequent crack lengths measured during propagation. The strain energy released between two crack length measurement points was calculated by the area of the triangle formed by these points and the origin (0,0), as depicted by the areas dU_1 and dU_2 in Fig. 3 [37]. The acoustic energy released between two crack length measurements was obtained by the sum of the energies of all hits detected in this interval, as depicted by dE_1 and dE_2 in Fig. 3.

The crack was propagated until 50 mm length, measured every

$$dE = \sum_{i=1}^{k} e_i$$

k = number of hits detected between two crack length measurements
e$_i$ = energy of a single hit
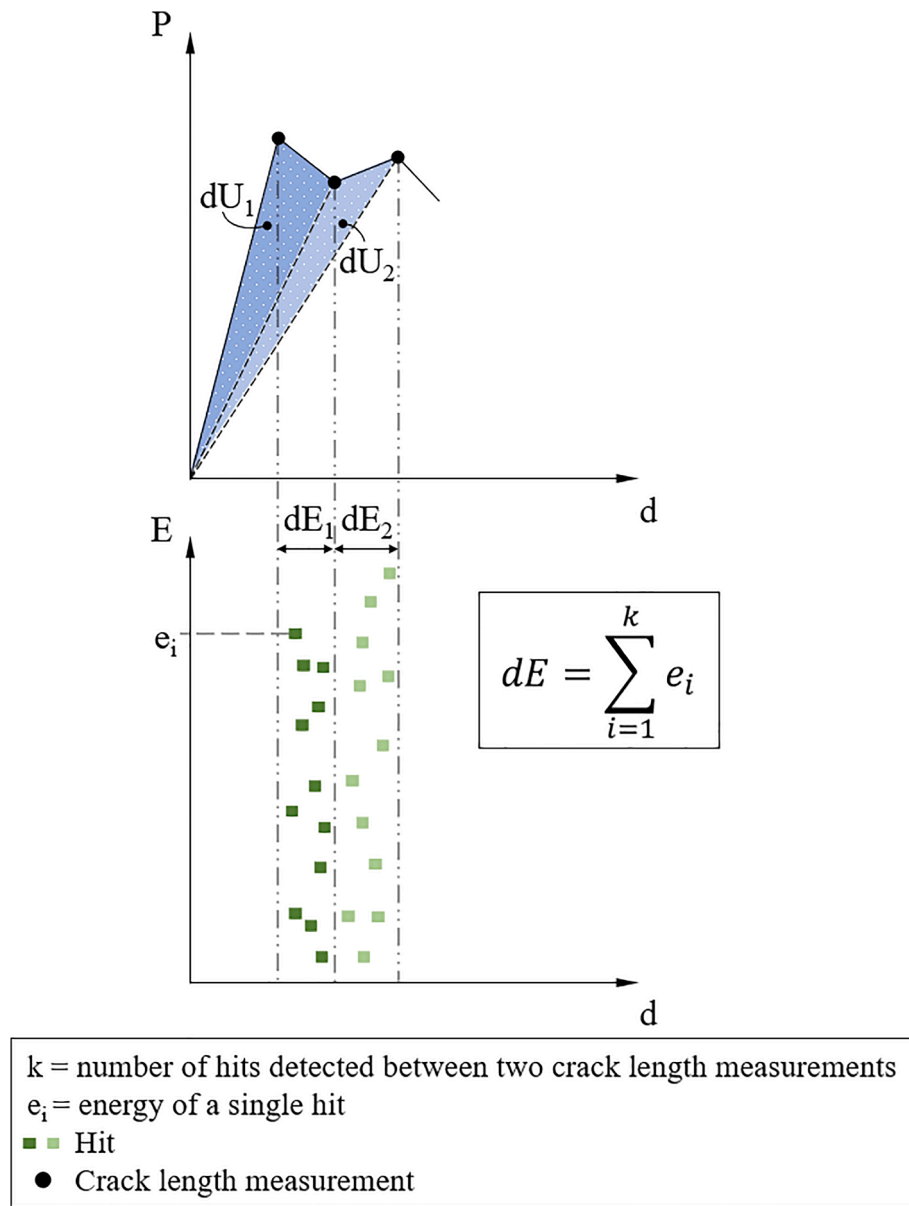■ ■ Hit
● Crack length measurement

Fig. 3. Concept of correlating the strain and the acoustic energy released between two subsequent crack length measurements.

millimeter (±0.13) from the starter crack tip. The release of quasi-static strain energy is proportional to fracture surface increments and therefore constant when a fixed crack length increment is considered. This allows discretizing the data to different crack increments. Here, $da = 0.5$ (through linear interpolation), 1, 2, and 3 mm were selected, and an average value for both energy measurements associated with a constant crack length increment was calculated, as illustrated in Fig. 4.

2.3.2. Fatigue delamination propagation

The concept of damage propagation releasing both strain and acoustic energy under quasi-static loading is also valid under cyclic loading conditions. However, instead of defining a fixed step of the crack tip to measure both energies, a fixed number of cycles was considered, in which both energies released were recorded, as illustrated in Fig. 5.

The fatigue tests were performed in displacement control, in which load, strain energy, and crack growth rate are at their maximum at the beginning of the test and gradually reduce insofar as the damage progresses. The increase of the specimen's compliance ($C = d/P$) and the reduction of P_n to $P_{n+\Delta n}$ after a period of $n + \Delta n$ cycles means that a fraction of the total strain energy (dU_{tot}) stored in the specimen was

released, considering there is no overlap in the hysteresis curves. This strain energy released corresponds to the area (dU_{tot}) highlighted in the P versus d chart presented in Fig. 4. In addition, the acoustic emission energy could be measured because the hits are synchronously recorded with the fatigue machine's data acquisition system, including time, displacement, and load. Therefore, each hit belongs to a defined cycle, and the acoustic energy released in the course of one cycle or a sequence of cycles can be easily quantified by the summation of each hit's energy, as presented in Fig. 5.

Literature shows evidence that the crack propagation rate affects the strain energy release [37,62]. Additionally, longer crack lengths obtained during fatigue tests lead to more fiber bridging, which might affect the release of both energies. Therefore, to minimize the influence of the da/dN and the fiber bridging on the results, only the fatigue tests' first 500 cycles were considered in the analyses, and their influence on the results was evaluated separately by reducing the maximum displacement (FT4 and FT5) and changing the pre-crack length (FT1-2 and FT1-3) in additional tests, respectively.

The analysis within 500 cycles was carried out with four different measurement ranges, i.e., intervals of 50, 100, 250, and 500 cycles. For
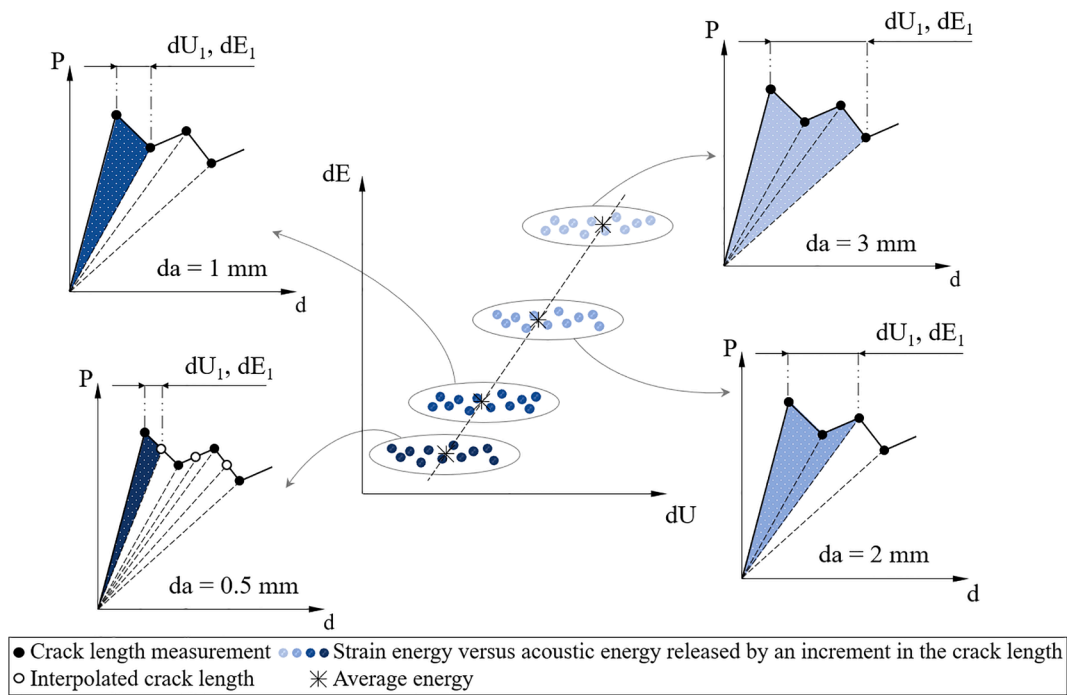
Fig. 4. Four different crack tip increments used to calculate the average values of strain and acoustic energies released in quasi-static loading.
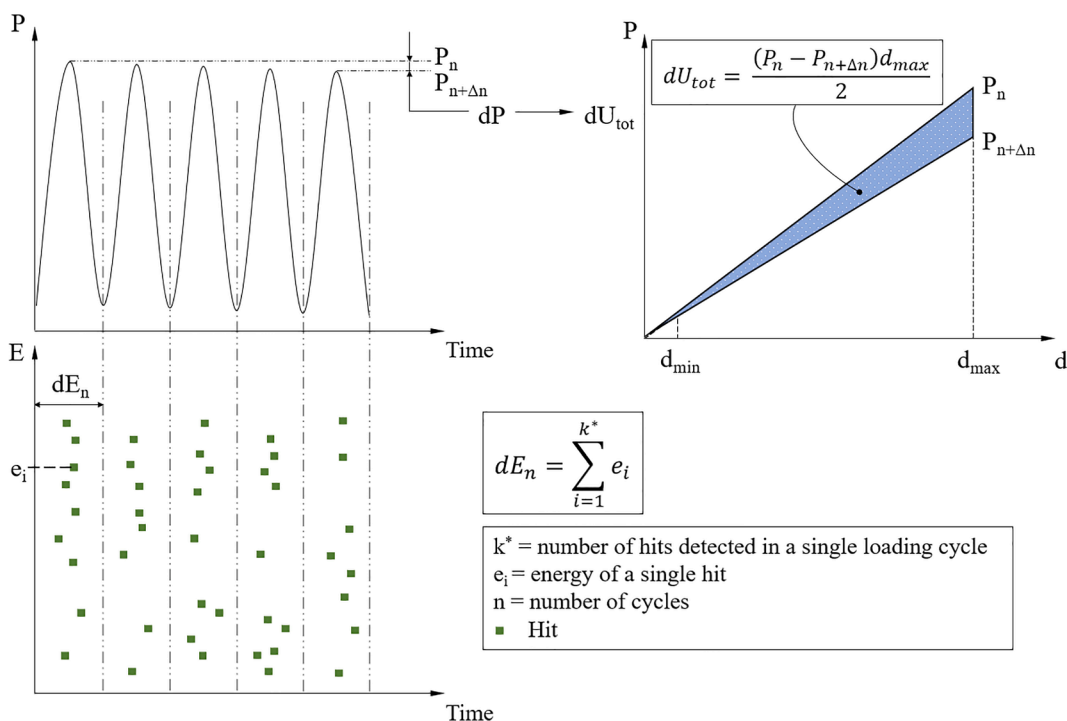

Fig. 5. Concept to correlate the strain and the acoustic energy released within a loading cycle sequence.

example, using the 50 cycles interval, the strain and the acoustic energies released were calculated every 50 cycles until it reaches 500 cycles, resulting in ten data-points for the plot dE versus dU (since only the total strain energy is considered, dU_{tot} will be referred to dU). The data-points obtained from the four measurement intervals adopted were plotted in a dE versus dU chart, as illustrated in Fig. 6.

2.4. Quantification of damage features on the fracture surfaces using scanning electronic microscopy (SEM)

The fracture surfaces created by crack propagation contain specific features that can elucidate damage mechanisms in materials. These damage mechanisms are the sources of acoustic signals [49] and relate to strain energy dissipation [37]. Therefore, the correlation between the fracture surface features, the acoustic energy release, and the strain energy release was investigated in this work. The methodology to
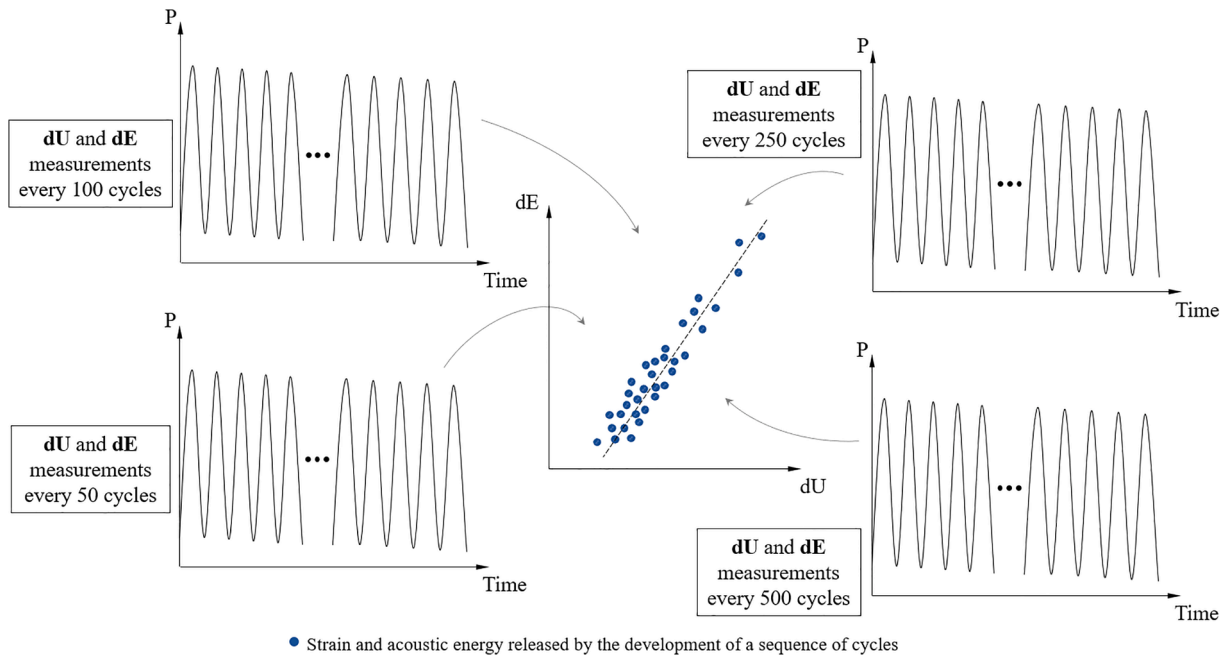
Fig. 6. Illustration of four different intervals of cycles considered to determine the dE versus dU curve in fatigue.
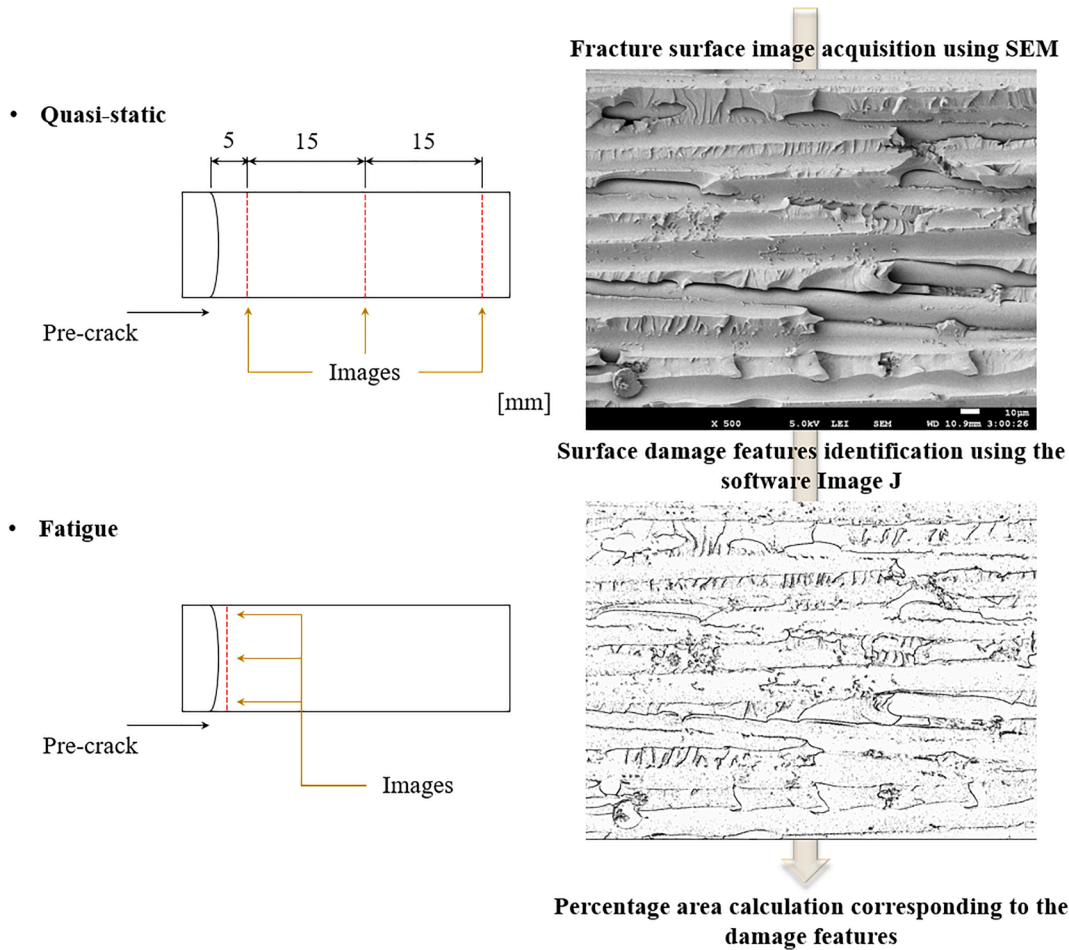

Fig. 7. Methodology to quantify the fracture surfaces in quasi-static and fatigue loading - percentage area = (black) / (black + white).

quantify the fracture surfaces' damage features is presented in Fig. 7.

The fracture surfaces of one specimen of each loading condition were investigated with SEM. Three images of each specimen's fracture surface were obtained with a constant magnification of 500x and an acceleration voltage of 5 keV, as indicated in Fig. 7. The fracture surfaces were covered with a 15 nm gold layer before SEM analysis. The fatigue test images were taken next to the pre-crack because only the first 500 cycles were considered in the AE analysis. The fracture surface patterns, e.g., river marks, scarps, fiber imprints, and hackles, were highlighted using the software Image J, following the procedures described in [63] and [64]. A new image containing only the edges corresponding to the damage features was generated (illustrated in Fig. 7), and the percentage area covered by these edges (area covered by black) was measured, quantifying the damage features on the fracture surface. Using this methodology enables quantitative comparisons between fracture surfaces originated from specimens tested under different load conditions rather than the usual qualitative analysis. The goal here is to observe whether the da/dN variation during the fatigue tests affects the marks on the fracture surface, indicating a variation in the number of damage mechanisms activated in the propagation process. However, this technique cannot identify or count specific damage mechanisms, which is not a problem since the goal here is finding a trend between the results rather than developing a model.

2.5. Measurements of the strain energy released within the loading cycle

The measurement of the strain energy released within a single loading cycle is not possible using the methodology described in Section 2.3 since this approach calculates the strain energy released based on the reduction of d_{max} after a sequence of cycles. The AE technique was used for this purpose, and conversion factors between acoustic and strain energies were determined from the correlations established using the methodologies described in Sections 2.3.1 and 2.3.2. The loading cycle was segmented into 22 equal displacement partitions (Δd), ensuring the same amount in both loading and unloading stages, to analyze the strain energy release distribution along the cycle, as depicted in Fig. 8. The division of the loading cycle into a different number of segments was evaluated, but the division into 22 segments was defined as an optimum value to provide enough details regarding the strain energy release distribution within the cycle.

The crack propagation in laminates does not occur as a uniform step of the crack front. Instead, various local extrusions are formed at the crack front, as observed by Brunner *et al.* [65]. These local damage events along the crack front do not affect the specimen's overall compliance because that relates to the overall crack length increment along the entire specimen width, which is obtained through the summation of several local extrusions. Hence, in fatigue, the strain energy release is an average measured phenomenon since it can only be determined when any variation in the compliance is detected after the development of several cycles. However, the local extrusions are sources of acoustic waves [65], which means that AE hits can be measured while the impact of each local extrusion on the specimen's compliance is too small to be captured. Therefore, to compare the strain energy release with the AE energy, the hypothesis is that AE measurements must be averaged (or accumulated) over multiple cycles.

Following this concept, the hits detected during the 500 loading cycles were overlapped and attributed to a segment according to displacement and time scales. The displacement scale was used to place the hit within the corresponding displacement range, while the time scale was used to define either the hit was detected during loading or unloading sections of the cycle. The total strain energy released in a single segment of the cycle was calculated by the summation of the corresponding hits' energies, followed by converting the acoustic energy into the strain energy using a conversion factor (Section 3.1). Finally, the total strain energy of each segment was plotted in a diagram (U versus Cycle segments), as illustrated in Fig. 8.

3. Results and discussions

3.1. Correlating strain (U) and acoustic i energies released due to delamination propagation

Before restricting the discussions to the correlation between both energies, the presentation of the results starts with the fracture surfaces analyses in Section 3.1.1, aiming to establish correlations between the fracture surface features, the strain energy release, the acoustic energy release, and the crack growth rate. These correlations are essential to explain the interactions between strain and acoustic energies presented in Sections 3.1.2 and 3.1.3, where the conversion factors were defined and later applied to measure the strain energy released within the loading cycles in Section 3.2.

3.1.1. Fracture surface analysis

The specimen's fracture surfaces were selected to evaluate the most extensive crack growth rate range possible (restricted to the crack propagation developed within 500 cycles). Then, the da/dN influence on the fracture surface's roughness was investigated. Fig. 9a, 9b, 9c, and 9d present the fracture surfaces of the specimens QS3, FT3, FT8, and FT5, respectively. Additionally, Fig. 9e and 9f show images of the fracture surfaces of specimen FT1 taken after 500 cycles, aiming to obtain images associated with lower da/dN.

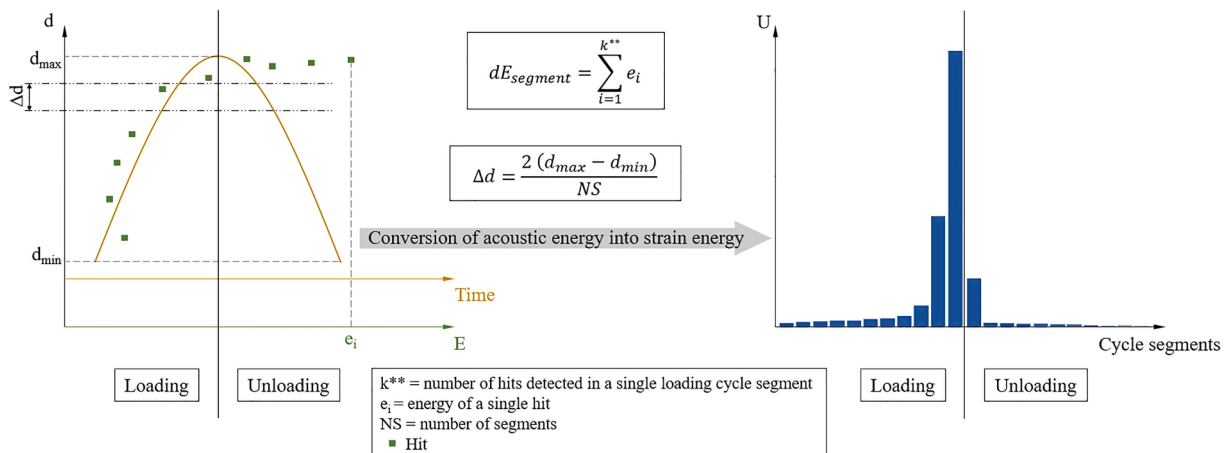The primary mechanisms observed on the fracture surfaces were the

Fig. 8. Detailed methodology used to assess the strain energy release distribution within the loading cycles.
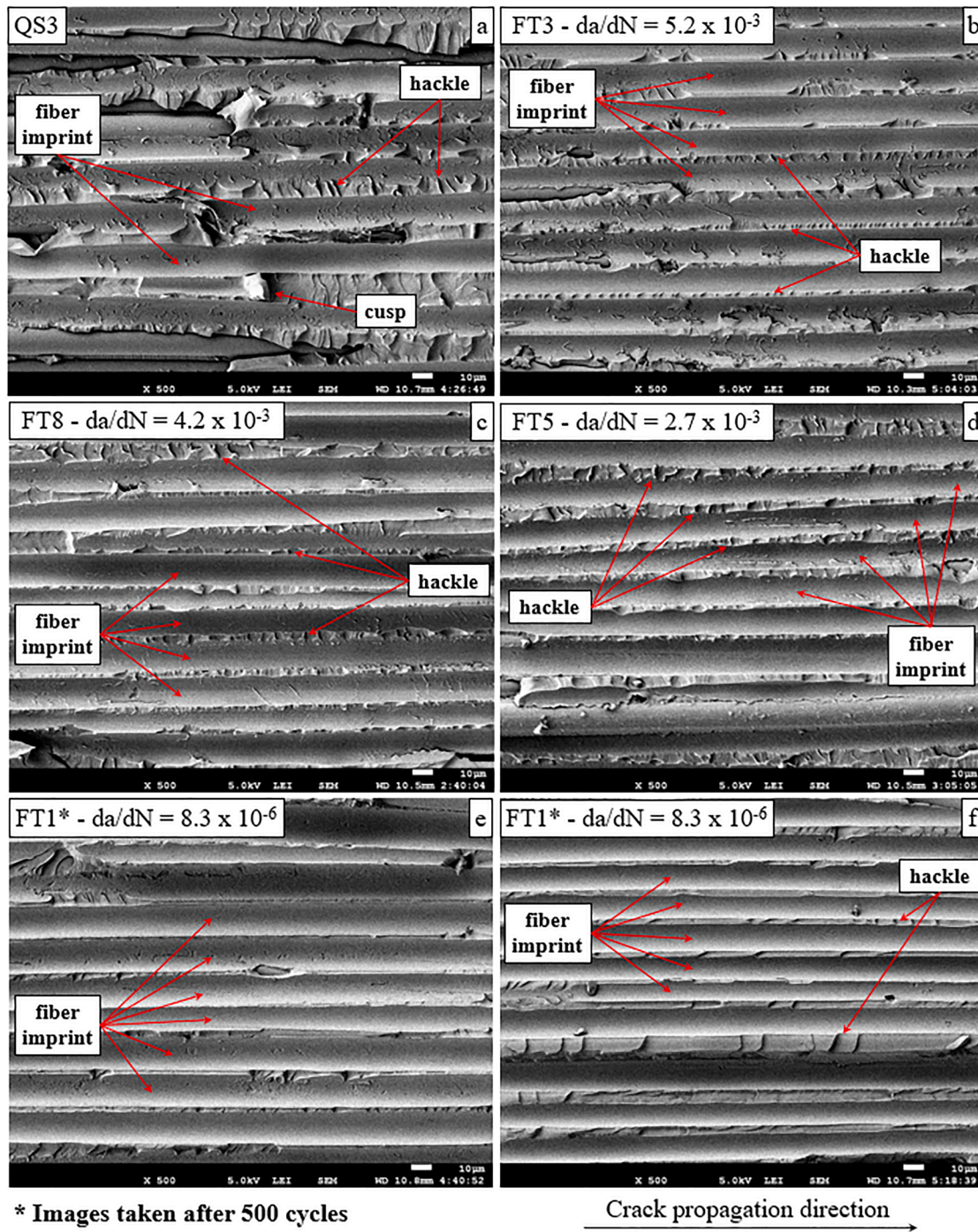
Fig. 9. Fracture surfaces with their corresponding crack propagation rates in millimeters per cycle (mm/cycle).

fiber imprints with hackles in between them. Besides that, the quasi-static specimens presented cusp patterns (see Fig. 9a), while the damage features found in the fatigue specimens were restricted to hackles and fiber imprints (see Fig. 9a, 9b, 9c, 9e, 9f), indicating a lower energy dissipation compared to the quasi-static propagation. Additionally, the fatigue specimens with low crack propagation rate (Fig. 9e and 9f) were governed by fiber imprints with fewer hackles, which also indicates lower energy dissipation. Some marks inside the fiber imprints can be observed in most images due to the cohesive failure of the fiber/matrix interface. The glass fibers used in this research work present a silane layer at their surface, leading to a strong interaction of the fibers with the epoxy resin, which explains the cohesive failure observed. Amaral *et al.* [37] used the term surface roughness to qualitatively describe the

number of damage features, in which higher roughness means a higher amount of damage marks on the surface. In Fig. 9, it is possible to note a rougher fracture surface in specimen QS3 (Fig. 9a) compared to the specimens tested in fatigue and a roughness reduction due to the *da/dN* reduction in the fatigue specimens.

The marks on the fracture surfaces are a consequence of damage events responsible for dissipating strain and acoustic energies. Hence, a fracture surface containing a high number of damage marks (or high "roughness") should be associated with high energy dissipation, according to the fundament of energy conservation [66]. In order to prove this hypothesis, Table 2 quantifies the damage marks on the fracture surfaces and associate these results with the average acoustic and strain energy released per area due to crack propagation after 500 cycles.

Table 2
Quantification of the damage features on the fracture surfaces - quasi-static and fatigue loading conditions.

Specimen	da/dN (mm/ cycle)	Average Edges' area (%)	STD deviation	dU/dA ($\times 10^5$ mJ/m^2)	dE/dA ($\times 10^{12}$ aJ/m^2)
QS3	–	10.88	0.7	2.98	1.81
FT3	5.24×10^{-3}	8.98	0.3	2.62	0.52
FT8	4.20×10^{-3}	8.73	0.17	2.58	0.49
FT5	2.66×10^{-3}	8.45	0.12	2.06	0.31
FT1*	8.33×10^{-6}	6.03	0.28	–	–

* **Measurement from images taken after 500 cycles.**

Additionally, the strain and acoustic energy release of specimen QS3 were calculated using the methodologies described in Section 2.3.1 and considering a crack propagation length of 4 mm (crack length comparable to the lengths obtained in the fatigue tests after 500 cycles).

The results presented in Table 2 show a higher surface area percentage covered by damage patterns in quasi-static conditions than in fatigue, which means a rougher fracture surface. The presence of more damage patterns in quasi-static loading correlates with the higher release of strain and acoustic energies in quasi-static propagation than in fatigue. The cyclic energy (driving force) applied to the specimen in fatigue leads to a reduction of the minimum energy required to damage onset compared to quasi-static conditions. In other words, the material resistance to crack propagation reduces under cyclic loading (propagation under lower G), which means less energy is released to create new fracture surfaces (lower dU/dA), as presented in Table 2.

A reduction of the area fraction corresponding to damage patterns was observed as long as the crack growth rate reduced in fatigue. However, this roughness reduction was not so sharp considering only the specimens FT3, FT8, and FT5 (images taken within 500 cycles) due to the short da/dN range covered by them, which led to a slight reduction of dU/dA and dE/dA, as depicted in Table 2. Thus, the results presented in Table 2 and Fig. 9 indicate that the da/dN reduction is associated with a reduction of both dU/dA and dE/dA, resulting in a "smoother" fracture surface, which suggests that the strain and acoustic energy release depends on the damage state of the fracture surface, as stated in the work of Amaral et al. [37].

As mentioned earlier, AE activity is associated with damage events developed during crack growth. Therefore, the reduction of the acoustic energy released at lower crack growth rates might be associated with the activation of less damage mechanisms, which can be translated into lower AE activity. On the other hand, the reduction of the acoustic energy released at lower crack growth rates might be associated with acoustic emissions with lower energy when damage mechanisms of the same nature are considered. However, this work cannot evaluate the veracity of these hypotheses with the results presented, and this topic must be evaluated in future works.

3.1.2. Quasi-static and fatigue delamination propagation

The strain and acoustic energy released were plotted against each other for quasi-static loading and for fatigue loading at two different R-ratios to reveal the influence of the load condition on the correlation between both energies.

The correlation of the strain energy release (dU) with the acoustic energy release (dE) is presented in Fig. 10. Fig. 10a, 10b, and 10c present the individual results of the specimens tested at each loading condition, while Fig. 10d presents a comparison between these three conditions. A linear curve that passes through the origin (0,0) was fitted to the experimental data with good agreement in the analyses because dU and dE both are zero when no damage is developed.

The results presented in Fig. 10 show a distinct behavior of the curves obtained from quasi-static and fatigue loading conditions. The linear curve fitted to the quasi-static data exhibits a considerably higher slope than the curves fitted to both fatigue data, see Fig. 10d. This slope increase indicates that if both loading conditions present a similar strain energy release due to damage propagation, more acoustic energy would be released under quasi-static than in cyclic load conditions. Facing these results, one could argue that energy release is proportional to
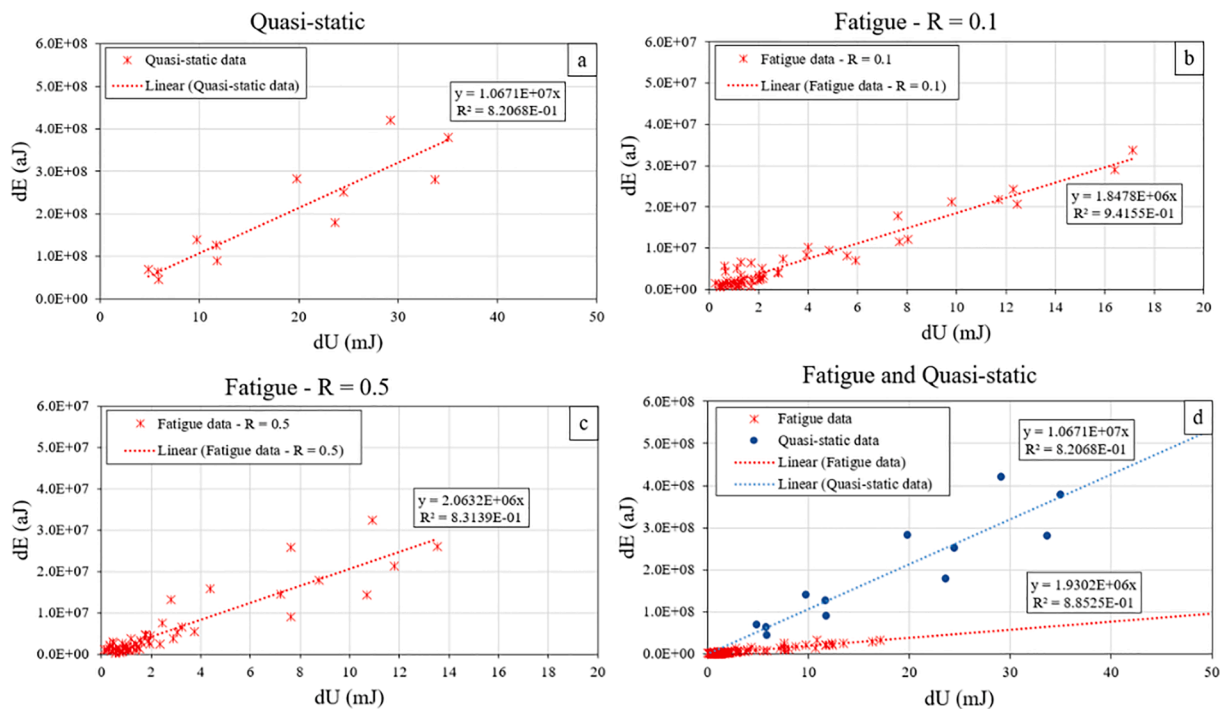

Fig. 10. Correlation of strain (dU) and acoustic (dE) energies released: (a) quasi-static loading – specimens QS1, QS2, and QS3; (b) fatigue loading (R = 0.1) – specimens FT1, FT2, and FT3; (c) fatigue loading (R = 0.5) – specimens FT7, FT8, and FT9; (d) comparison between quasi-static and fatigue results.

damage, and a variation in the loading condition should similarly affect the release of both energies. Indeed, the activation of more damage mechanisms increases the release of both acoustic and strain energy, as already observed in Section 3.1.1. However, it does not mean that the release of both energies should increase at the same proportion keeping a constant slope under different loading conditions.

The acoustic energy and the strain energy have distinct natures. The acoustic signals result from a sudden displacement caused inside the material when any damage mechanism is developed [49], while the strain energy is released due to a compliance increase when damage propagates. Hence, it is intuitive that different damage mechanisms might affect the release of each energy differently. Furthermore, the acoustic emission is very sensitive to distinct damage mechanisms. For example, the rupture of fibers is usually associated with high energy dissipation, while a crack in the matrix dissipates relatively low acoustic energy [61,67–69]. Therefore, the presence of fiber breakage during damage propagation might cause a substantial impact on the acoustic energy release, while the strain energy is less affected. In the present work, the main reasons for the acoustic energy release increase during quasi-static propagation are the fiber bridging formation and the presence of unstable crack propagation.

The development of crack tip jumps, i.e., a sudden increment of the crack length along the entire specimen's width (Δa), is characteristic of an unstable crack propagation. These jumps lead to a considerable release of acoustic energy (ΔE) and a sudden variation of the specimen's compliance, resulting in a sudden load reduction [70], as observed in the curves plotted in Fig. 11.

Fig. 11 presents the crack length increment (Δa) and the acoustic energy release (ΔE – calculated following the methodology described in Section 2.3.1) related to three of the crack tip jumps detected during the quasi-static tests. The acoustic energy released due to these jumps was substantially higher than the one observed in fatigue (steady crack propagation), in which the average acoustic energy released in the tests with $R = 0.1$ and $R = 0.5$ was 1.13 (± 0.14) $\times 10^7$ aJ/mm and 1.07 (± 0.24) $\times 10^7$ aJ/mm, respectively. Moreover, the instability related to quasi-static propagation leads to a natural scatter of the results, as observed in Fig. 10, in which the scatter of the quasi-static results (Fig. 10a) was considerably higher than in fatigue (Fig. 10b and 10c).

The fiber bridging was another factor that contributed to a higher

acoustic energy release in quasi-static propagation than in fatigue. The quasi-static tests were conducted until a 50 mm crack length (not considering the pre-crack), while the fatigue tests accounted for a crack length no longer than 4 mm (considering only the first 500 cycles). Consequently, a considerably higher displacement was reached in quasi-static than in fatigue tests. The longer crack length increases the amount of fiber bridging, and the higher displacement results in the failure of some bridged fibers (fiber breakage or fiber pull-out from the matrix), mechanisms associated with high acoustic energy dissipation.

The analyses presented in Section 3.1.1 indicated an increase in the damage mechanisms activated during quasi-static loading compared to fatigue, e.g., more plastic deformation through hackle formation, more cracks into the crack plane, more matrix cleavage, and the rupture of more fibers [37], which contributed to increasing both the acoustic and the strain energy released (SER). However, the results showed a greater influence of these variables on the acoustic energy release than in the strain energy release, contributing to the higher slope of the quasi-static results observed in Fig. 10.

Regarding the fatigue results, the slope of the curve obtained for the *R*-ratio of 0.1 (Fig. 10b) was slightly lower than the slope for the *R*-ratio of 0.5 (Fig. 10c). In addition, the average da/dN of the specimens tested with $R = 0.1$ and $R = 0.5$ were 5.0 (± 0.7) $\times 10^{-3}$ mm/cycle and 4.4 (± 0.9) $\times 10^{-3}$ mm/cycle, respectively, calculated through the division of the total crack length after 500 cycles by the number of cycles. The *R*-ratio increase reduces the work applied to the specimen, leading to a da/dN reduction [71]. Hence, the *R*-ratio variation indirectly affects the correlation between the strain and acoustic energies through the variation of da/dN. The discussions concerning the influence of the da/dN on the correlation between acoustic and strain energy release are restricted to Section 3.1.3, where more results are presented, aiming to investigate a broader da/dN range.

The linear curve fitted to the data of strain and acoustic energies in Fig. 10 allows determining a conversion factor to obtain strain energy from acoustic energy, as illustrated in Fig. 12. Therefore, different slopes of the curves imply different conversion factors, as observed in the results presented in Fig. 10, and a conversion factor must be determined for each test condition.

The quasi-static tests analysis aimed to evaluate whether a conversion factor could be obtained from a standardized test procedure, i.e.,
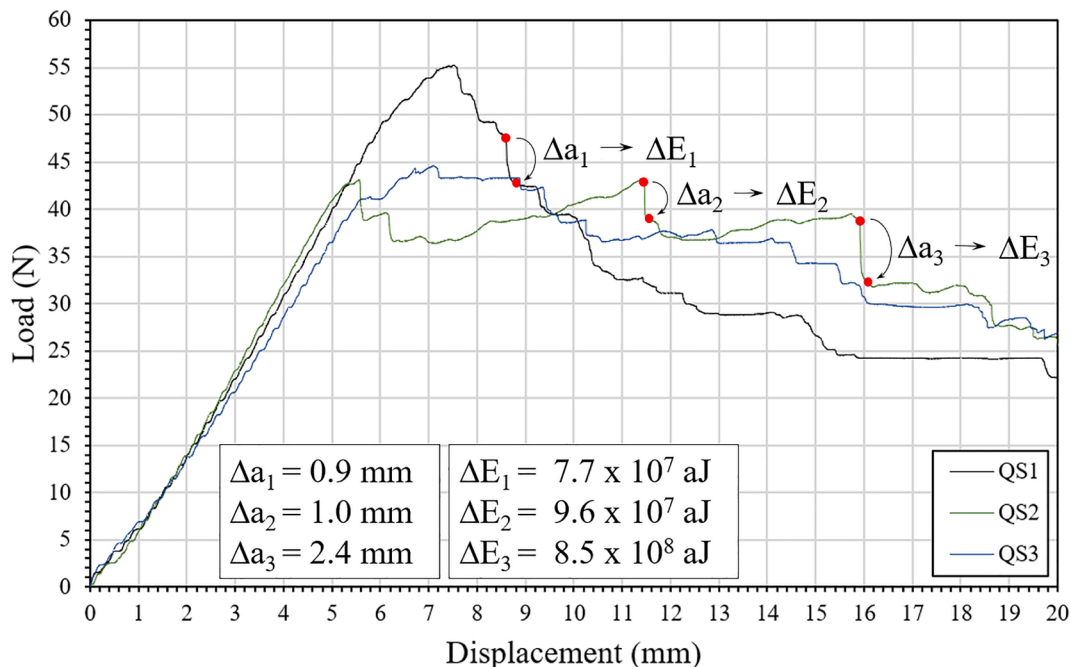

Fig. 11. Release of acoustic energy (ΔE) due to a sudden increment of the crack length (Δa).
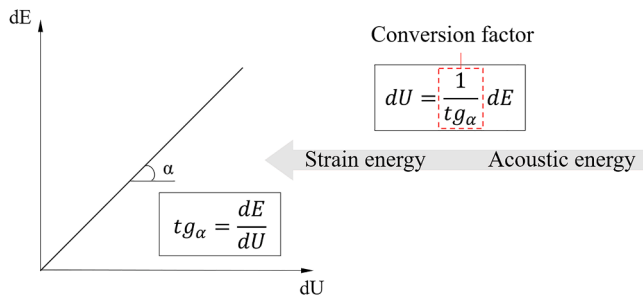
Fig. 12. Conversion factor obtained by the slope of the acoustic (dE) and strain (dU) energy release curve.

following the guidelines described in ASTM D5528-13 [56]. This revealed the influence of fiber bridging on the results when developed over a longer crack length. Therefore, the influence of fiber bridging in fatigue tests is analyzed in the next section by varying the crack length.

3.1.3. The effect of fiber bridging and crack growth rate on the release of strain and acoustic energies

The influence of the variation in the amount of fiber bridging on the correlations between both energies was investigated by testing the specimen FT1 in fatigue three consecutive times. The development of sequential tests means a longer crack length in each test, which explains the fiber bridging increase, see Fig. 13c. Fig. 13a presents the results of the tests performed with specimen FT1, while Fig. 13b compares the results obtained using long crack lengths (high fiber bridging content) with results obtained using the pre-crack length of 34 mm (low fiber bridging content).

All the test specimens developed some fiber bridging prior to the tests because of the process used to open the pre-crack length of 34 mm (see Section 2.2). Hence, there is a curve that represents the zero-bridging behavior, but it is hard to define or measure where this curve should be since it is almost impossible to avoid the presence of fiber bridging during propagation entirely. Some authors consider fiber bridging as an extrinsic mechanism and disregard their effect on the results [72,73]. In this work, the fiber bridging is considered an intrinsic phenomenon, which means the energy released due to the failure of bridged fibers is measured in the process along with other damage mechanisms developed during crack propagation [24].

In the case of low fiber bridging content, the release of strain and acoustic energies is mainly due to the crack tip's damage. For well-developed fiber bridging conditions, the damage developed is attributed to the crack tip and the region behind the crack tip. The presence of fiber bridging shields the crack tip, storing a fraction of the cyclic load applied to the specimen to be released during the unloading. When these bridged fibers fail, strain and acoustic energies are dissipated [39], increasing both *dU/dA* and *dE/dA*. High fiber bridging content increased the angular coefficient of the curves, as discussed in Section 3.1.2 and observed in the results presented in Fig. 13, which means a more significant increase in the acoustic energy release than the strain energy release due to the development of more events associated with high acoustic energy dissipation, e.g., fiber breakage.

To study the effect of crack growth rate on the correlation between strain and acoustic energies release, tests were performed with different d_{max} [74], as follows: FT4 with 90 % of d_{max}, FT5 with 85 % of d_{max}, and FT6 with 80 % of d_{max} (see Table 1). In Fig. 14, the obtained linear trends of specimens FT5 and FT6 present a very similar slope, while specimen FT4 presents a curve with a steeper slope, which implies that reducing the crack growth rate also reduces the slope. However, the results presented previously in Fig. 10 showed an opposite behavior, which obscures the definition of a trend between *da/dN* and the slope of the curves (conversion factor).

The absence of a clear trend of the results relies on the effect of *da/dN* on the release of strain and acoustic energies. The *da/dN* reduction not only reduces *dU/dA* but also originates a "smoother" fracture surface [37], which means that fewer damage events are associated with the fracture process when *da/dN* is reduced. These damage events are sources of acoustic waves, and the reduction of the damage events yields to a reduction of the acoustic energy released per area (*dE/dA*), which tends to reduce the curve slope. Therefore, the *da/dN* reduction results in two competing phenomena that affect the curve slope in opposite ways: the *dU/dA* reduction increases the slope while the *dE/dA* reduction reduces the slope. Hence, it is almost impossible to find a fixed trend between *da/dN* and the curve slope. Besides that, the scatter bands are increased due to the presence of extrinsic errors related to the measurement methodology and measurement systems (AE system and fatigue machine), and intrinsic errors associated with inhomogeneities of the material and fiber bridging, inhibiting the observation of a clear trend between the *da/dN* and the curve slope [24].
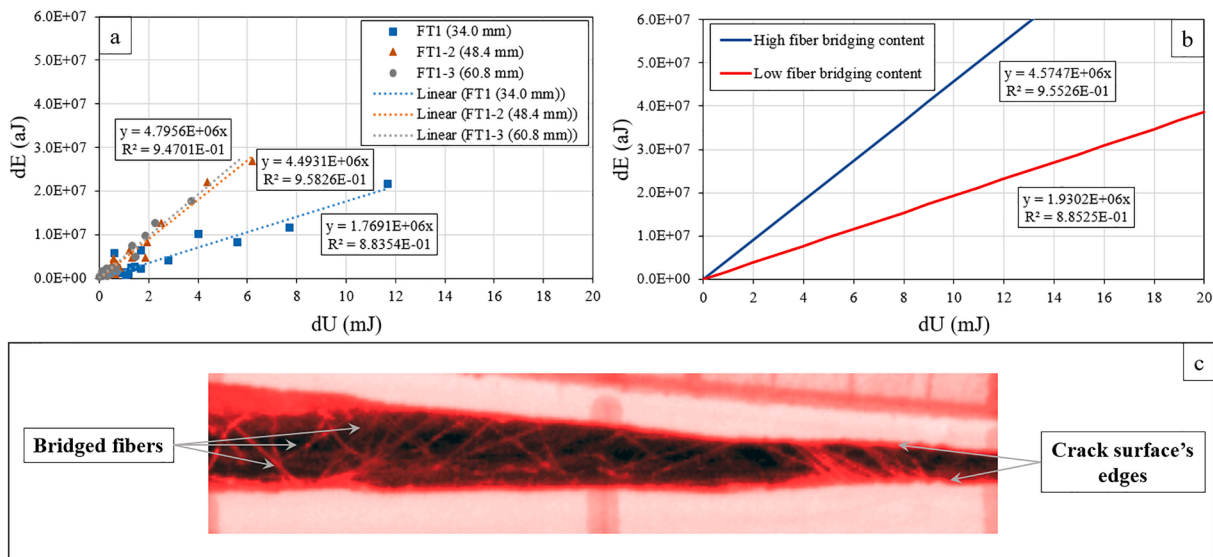

Fig. 13. Correlation of strain (dU) and acoustic (dE) energies released in FDG (R = 0.1): (a) varying pre-crack lengths; (b) comparison between high (FT1-2 and FT1-3) and low bridging content (FT1, FT2, FT3, FT7, FT8, and FT9); (c) fiber bridging development.
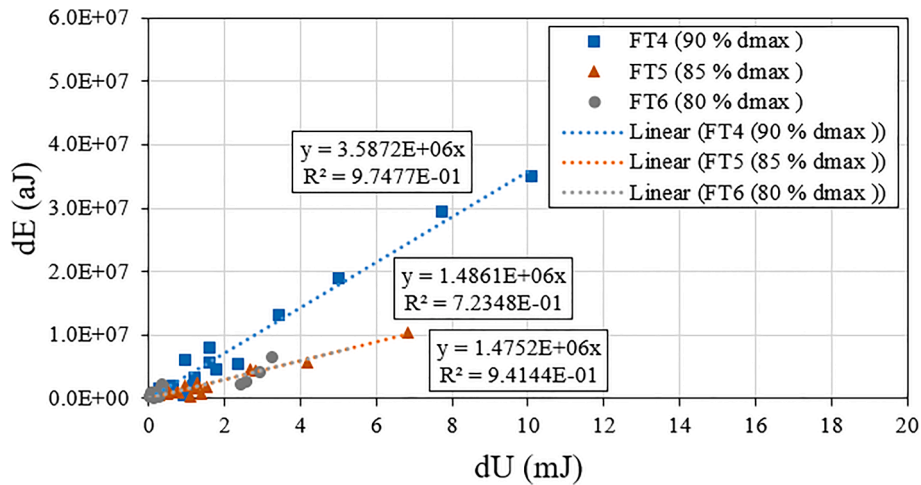
Fig. 14. Correlation of strain (dU) and acoustic (dE) energies released in FDG varying dmax with R = 0.1.

3.2. Strain energy release within the fatigue loading cycles

The results in Section 3.1 allow the use of the correlation between strain and acoustic energy to evaluate the strain energy release distribution within the fatigue cycles from the acoustic energy release measurements through a conversion factor. However, the obtained conversion factor depends on the loading conditions, which means that a different conversion factor must be calculated to each loading condition. Furthermore, the AE has bridging in it, not only crack increment. Hence, the energy release surrounding d_{max} (cycle region where the bridging effect is maximum) might increase due to the release of energy when the bridged fibers break or pull out from the matrix.
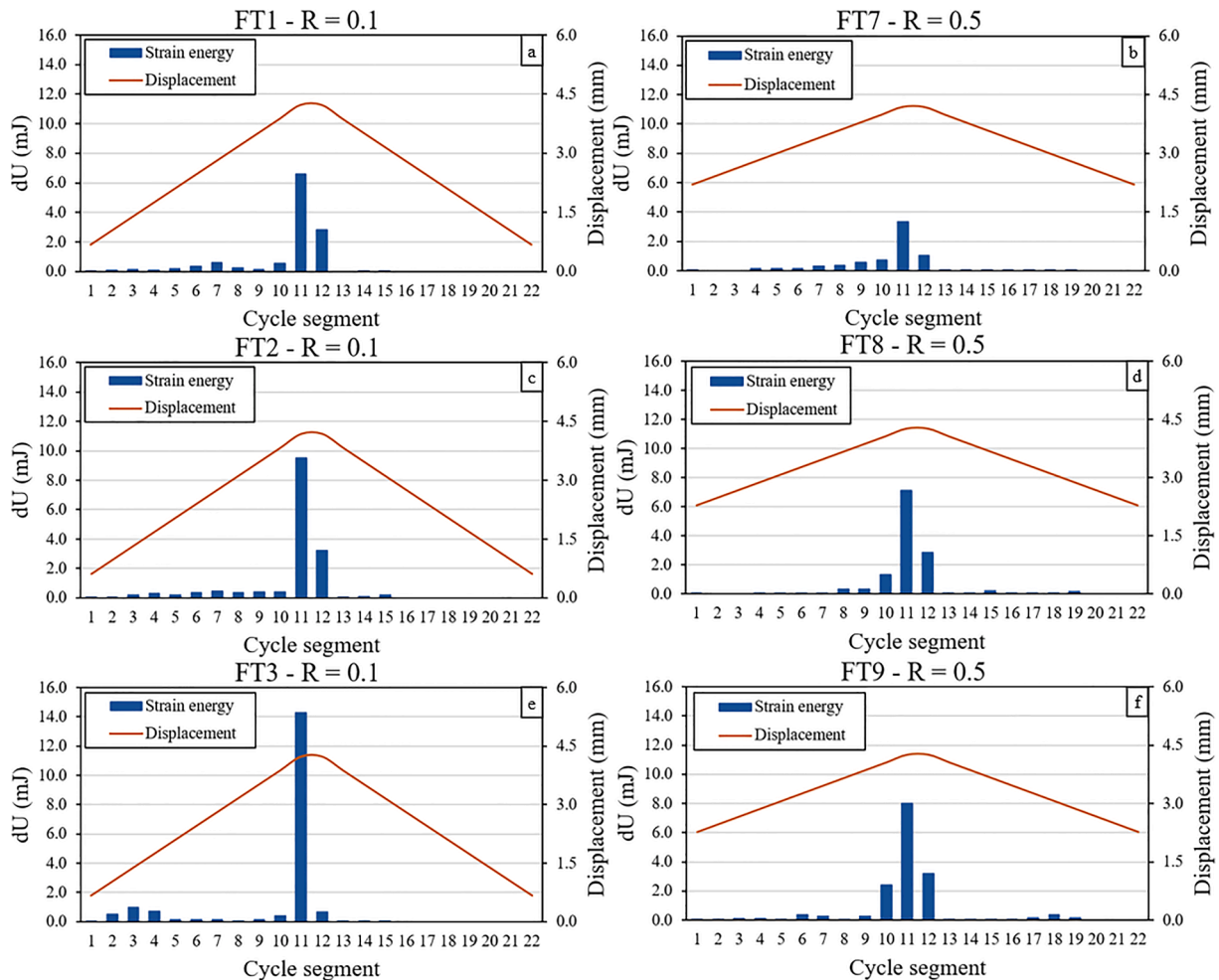
* The displacement variation was sinusoidal, which is not possible to observe because the displacement was plotted against the cycle segments.

Fig. 15. Distribution of the SER within the loading cycle calculated from the acoustic emission detected over 500 cycles with the R-ratios: 0.1 and 0.5.

Fig. 15 presents the strain energy release distribution within the loading cycle calculated from the acoustic emission detected over 500 cycles. The specimens tested with $R = 0.1$ and $R = 0.5$ had the strain energy release calculated from AE measurements using the conversion factors obtained in Section 3.1.2 in Fig. 10b and 10c, respectively.

The results of all specimens in Fig. 15 show a high SER concentration surrounding d_{max}, despite the R-ratio applied. In other words, the SER rate increases when the specimen is under a high strain energy accumulation state. Comparing the SER distribution of specimens tested with both R-ratios, it is possible to note a higher concentration of SER surrounding d_{max} (segment 11) in the specimens tested with an R-ratio of 0.1 (Fig. 15a, 15c, and 15e) than an R-ratio of 0.5 (Fig. 15b, 15d, and 15f). This higher energy release concentration is mainly due to the data presentation methodology instead of the material behavior itself. The R-ratio increase reduces the displacement range within a single cycle, but the cycle was still divided into 22 segments, reducing the displacement range of each segment. Therefore, it is expected to observe an apparent reduction in the SER concentration surrounding d_{max} when the R-ratio increases.

The displacement increases gradually in the loading process, increasing the strain energy stored in the specimen until its maximum at d_{max}, the moment in which more energy is available for damage propagation. However, new fracture surfaces will only be created, releasing part of this energy, if the driving force is equal or higher than the material resistance to damage formation, referred to as U_{th} in this work [32,42]. The results in Fig. 15 present evidence of damage formation in the early stages of the loading cycle, which could mean that almost the entire cycle was in an energy state above U_{th}, leading to one crucial question: **if the driving force is above U_{th} in the early stages of the cycle, why is the damage propagation concentrated around d_{max}?**

The answer relies on the multiple damage mechanisms associated with the fatigue crack propagation in FRPs, e.g., matrix cracking, failure in the interface fiber/matrix, fiber breakage, and delamination. Each damage mechanism requires a characteristic amount of energy to occur (different U_{th}) [42], which implies that each of them is activated in a specific region of the cycle when a certain energy threshold is crossed. Therefore, a single energy threshold (U_{th}) to predict damage onset within a single loading cycle is not suitable. Fig. 16 shows how the presence of different U_{th} affects the strain energy release within the loading cycle.

In Fig. 16, the SER measured over 500 cycles was overlapped and assessed as a single loading cycle, representing an average behavior of these cycles. Additionally, the total strain energy released after 500 cycles was calculated, and the SER distribution along the cycle from d_{min} until d_{max} was evaluated by the increments in the percentage of this total energy until it reaches 100 %, as depicted in Fig. 16a (loading) and 16b (unloading).

The damage onset for the specimens tested with $R = 0.1$ occurred when the displacement reached 1 mm (U_{TH1}), and the percentage of strain energy released increased at an approximately constant rate until it reached U_{TH2}, see Fig. 16a. Specimens tested with $R = 0.5$ started the cycles with d_{min} higher than U_{TH1}. Consequently, some damage mechanisms were already activated since the beginning of the cycles. From d_{min} until U_{TH2}, the specimens FT8 and FT9 presented a constant increase in the percentage of strain energy released, similar to the increase rate observed in specimens tested with $R = 0.1$, while specimen FT7 presented a higher SER rate. No clear energy threshold to activate a new damage mechanism was observed between U_{TH1} and U_{TH2}. However, it does not mean that all the damage mechanisms developed within this region were associated with U_{TH1}. The damage mechanisms between U_{TH1} and U_{TH2} have the feature of releasing low amounts of energy compared to the damage mechanisms activated above U_{TH2}, making it difficult to detect more threshold energy levels based only on the strain energy release behavior. Additionally, it is important to mention that few hits created due to friction might have been detected close to d_{min} during loading as damage-related signals, which may have caused a slight displacement of U_{TH1} towards the left in Fig. 16a and 16b. This possibility is restricted to specimens tested with $R = 0.1$ since d_{min} increases when the displacement ratio increases, reducing the friction between the fracture surfaces [42].
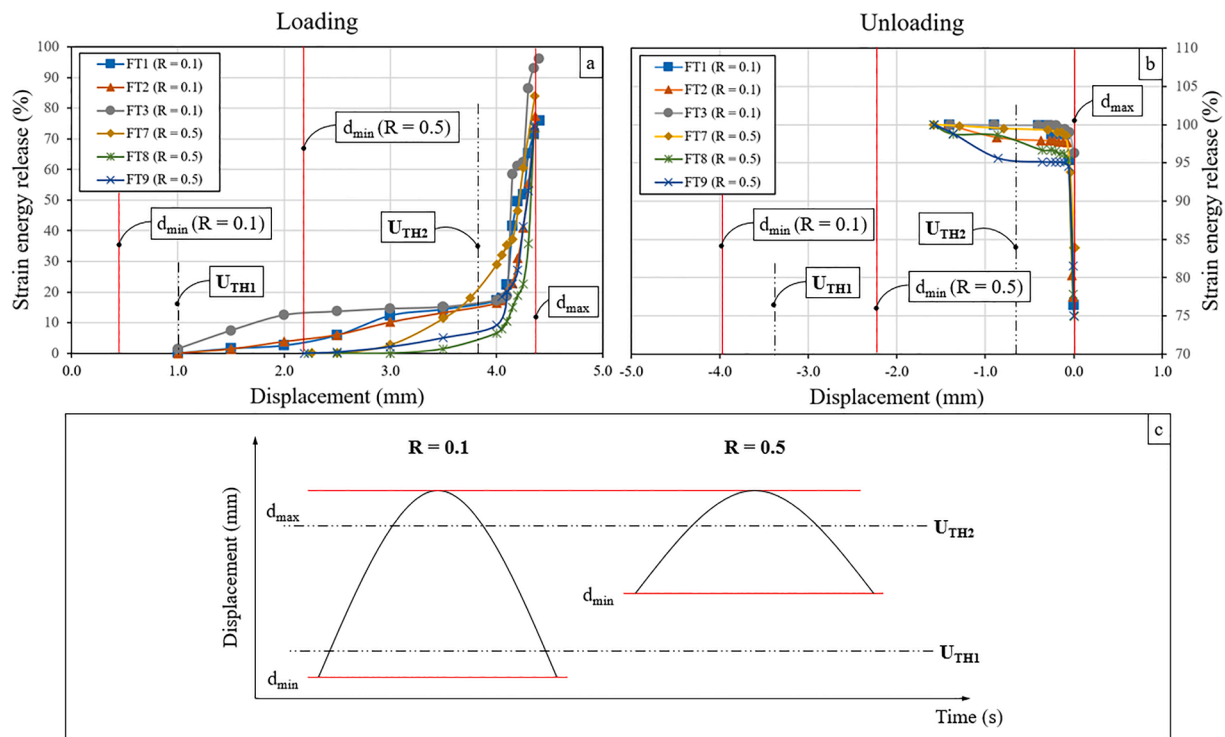

Fig. 16. Total strain energy released over 500 fatigue cycles within the loading cycle: (a) Loading; (b) Unloading; (c) time spent by the loading cycle above each energy threshold.

The specimens tested with both *R*-ratios presented a substantial increase in the SER rate shortly before the displacement reached 4 mm, showing that a new energy threshold was exceeded (U_{TH2}), activating new damage mechanisms. About 80 % of the strain energy released within the loading cycle occurred above U_{TH2}, composed of 60 % released during the loading process and 20 % released during the unloading process. After crossing U_{TH2} at the unloading, the specimens presented a low strain energy release until it stopped. The damage propagation at the unloading can occur as long as the energy available for damage propagation is above the energy threshold required to activate new damage mechanisms, which agrees with the results reported by Motta *et al.* [42] and Pascoe *et al.* [32].
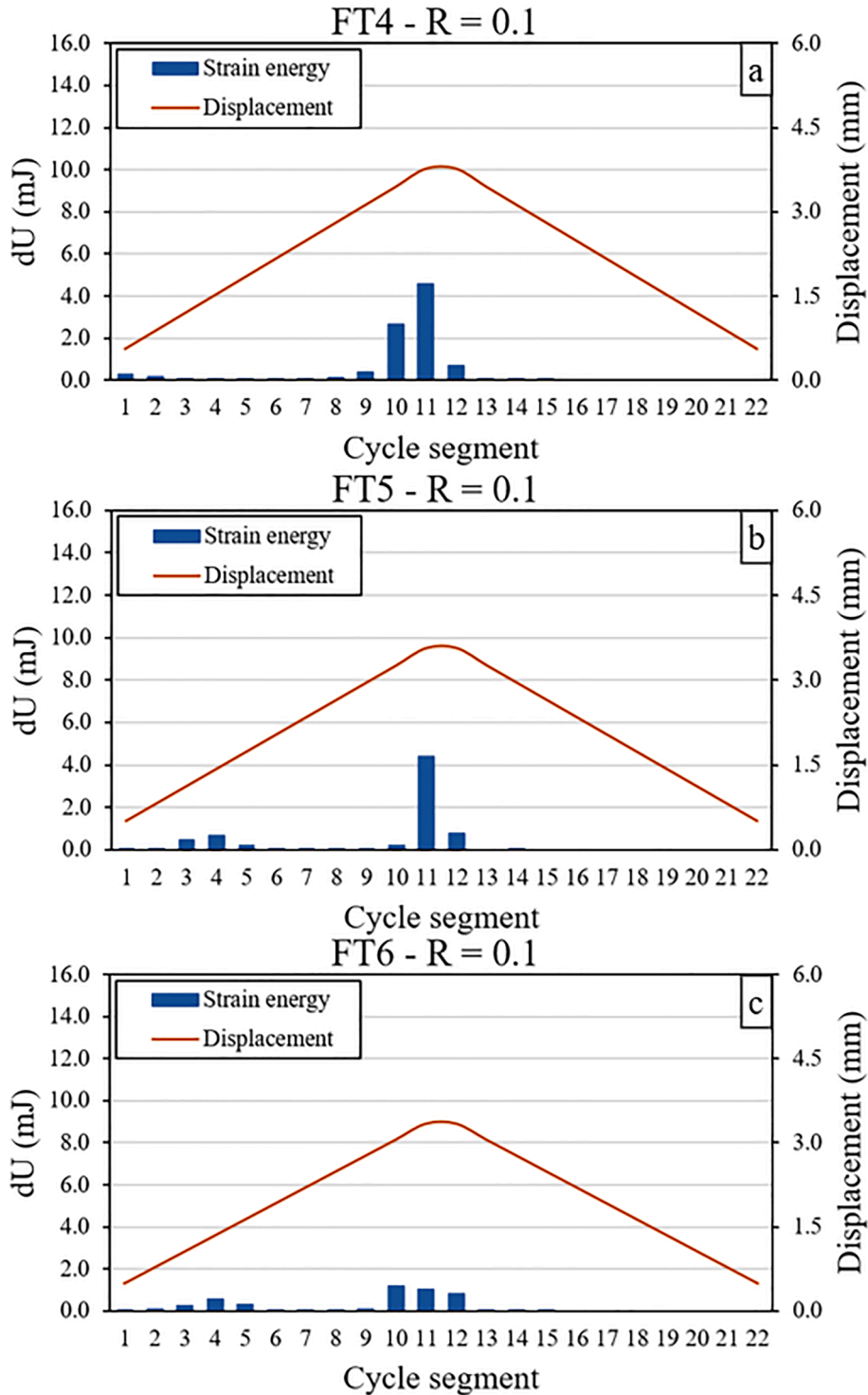
* The displacement variation was sinusoidal, which is not possible to observe because the displacement was plotted against the cycle segments.

Fig. 17. Distribution of the SER within the loading cycle calculated from the acoustic emission detected over 500 cycles with the R-ratios of 0.1 and a reduction of dmax.

The substantial energy released above U_{TH2} observed in Fig. 16 means that a reduction of d_{max} (an equal pre-crack length should be considered) until values close or even lower than U_{TH2} would reduce or inhibit the activation of some damage mechanisms, causing a massive reduction in the strain energy released. This behavior can be observed in the results of strain energy distribution within the loading cycles of specimens FT4 (d_{max} = 3.92 mm), FT5 (d_{max} = 3.71 mm), and FT6 (d_{max} = 3.49 mm) presented in Fig. 17a, 17b, and 17c, respectively.

Fig. 17c illustrates that the time spent by the loading cycle above each energy threshold increases when the *R*-ratio increases. Naturally, the first expectation facing this trend is the development of more damage, translated into an increase of dU/dN and da/dN. However, the average total strain energy released and the average final crack length calculated after 500 cycles presented a reduction of about 23 % and 11 % when the R-ratio increased from 0.1 to 0.5, respectively. Similar results were observed by Motta *et al.* [42], which reported a reduction in damage propagation when the *R*-ratio increased even with an increased time spent by the cycle above U_{th}.

In this research, U_{th} quantifies resistance to damage propagation as the minimum energy required to activate a specific damage mechanism and not as the energy dissipated due to damage propagation. Thus, damage will only propagate if the 'driving force' exceeds U_{th}. Consequently, the statement that the time spent by the loading cycle above each energy threshold increases when the R-ratio increases is valid only if the total strain energy (U or G_{max}) were the driving force. However, some authors have correlated the driving force with cyclic energy (U_{cyc}, $\Delta G = G_{max} - G_{min}$, or $\Delta\sqrt{G} = (\sqrt{G_{max}} - \sqrt{G_{min}})^2$) rather than total energy [28]. Following this hypothesis, the *R*-ratio increase with d_{max} kept constant would reduce the driving force, which means less energy available to damage propagation [42], explaining the lower propagation rate observed in specimens tested with $R = 0.5$. In other words, U_{th} is the minimum energy to activate a damage mechanism, while beyond that level, U_{cyc} (or ΔG) drives the crack, defining how much energy is available to be dissipated through crack growth. Therefore, in order to increase the fraction of the cycle above U_{th}, the driving force must be increased by increasing d_{max} or reducing the R-ratio. It is essential to mention that this research is focused on resistance, i.e., the definition of multiple energy thresholds, rather than driving force. However, the supposition that the driving force correlates with cyclic energy showed a good agreement with the results and must be evaluated in more detail in future works.

The presence of multiple energy thresholds means that the crack can propagate through the development of different damage mechanisms depending on which energy threshold is crossed within the loading cycle. The fact of the crack propagation being governed by distinct damage mechanisms depending on the loading cycle applied results in different resistances of the material to crack propagation (variation of dU/dA). The driving force determines whether the cycle is above a specific energy threshold or not. For example, the damage propagated while the driving force is higher than U_{TH2} releases more energy than the damage propagated while the driving force is between U_{TH1} and U_{TH2}. Therefore, one cycle with the driving force higher than U_{TH2} will present higher dU/dA than one cycle with the driving force between U_{TH1} and U_{TH2}.

It was previously verified that the dU/dA reduction due to a da/dN reduction originated "smoother" fracture surfaces. The presence of fewer damage marks on the fracture surfaces indicates the activation of fewer damage mechanisms, which is explained by a crack propagation with the driving force above different energy thresholds. The crack propagation under displacement-controlled conditions reduces the maximum load applied to the specimen at d_{max}, resulting in a gradual reduction of the driving force. Consequently, at some point during crack propagation, the driving force might become lower than some energy threshold, which means the damage mechanism associated with that energy threshold will no longer occur, e.g., the rupture of fibers restricted to high propagation rates [37], reducing dU/dA and the resistance to crack propagation.

4. Conclusions

This research presents a methodology that enables to measure the strain energy released within a single loading cycle in fatigue using the AE technique, leading to the following conclusions:

- The correlation between strain and acoustic energies is linear for the determined range of first 500 cycles, enabling the conversion of one energy into another, using a conversion factor calculated from the slope of the dE versus dU curve;
- This correlation depends on the fiber bridging content and the crack propagation rate. Therefore, a different conversion factor must be calculated to each load condition;
- FDG comprises different damage mechanisms with each a specific amount of energy to be activated; thus, there are multiple U_{th} within the loading cycle associated with distinct damage mechanisms;
- The strain energy released was concentrated near d_{max}, where the elastic strain energy stored in the specimen reaches its maximum, activating the highest number of damage mechanisms;
- FDG under displacement-controlled conditions gradually reduces da/dN due to the reduction of the energy available to damage propagation. Reducing the driving force means the activation of fewer damage mechanisms during crack propagation when fewer energy thresholds are crossed. Hence, less energy is released during propagation (dU/dA). In other words, the specimen's resistance to crack propagation in terms of dU/dA reduces because fewer damage mechanisms were activated. However, the multiple energy thresholds are a material property, and they are constant despite the load applied.

CRediT authorship contribution statement

Roberto Ferreira Motta: Conceptualization, Methodology, Validation, Formal analysis, Investigation, Data curation, Writing – original draft, Writing – review & editing, Visualization. **René Alderliesten:** Resources, Supervision, Project administration, Funding acquisition. **Dimitrios Zarouchas:** Methodology. **Marcos Yutaka Shiino:** Writing – review & editing, Visualization, Supervision. **Maria Odila Hilario Cioffi:** Project administration, Funding acquisition. **Herman Jacobus Cornelis Voorwald:** Project administration, Funding acquisition, Supervision.

Declaration of Competing Interest

The authors declare that they have no known competing financial interests or personal relationships that could have appeared to influence the work reported in this paper.

Data availability

Data will be made available on request.

Acknowledgement

References

[1] Pernice MF, De Carvalho NV, Ratcliffe JG, Hallett SR. Experimental study on delamination migration in composite laminates. Compos Part A Appl Sci Manuf 2015;73:20–34. https://doi.org/10.1016/j.compositesa.2015.02.018.

[2] Bhuiyan FH, Fertig RS. Predicting matrix and delamination fatigue in fiber-reinforced polymer composites using kinetic theory of fracture. Int J Fatigue 2018; 117:327–39. https://doi.org/10.1016/j.ijfatigue.2018.08.007.

[3] Drake DA, Sullivan RW. Prediction of delamination propagation in polymer composites. Compos Part A Appl Sci Manuf 2019;124:105467. https://doi.org/10.1016/j.compositesa.2019.05.035.

[4] Simon I, Banks-Sills L, Fourman V. Mode I delamination propagation and R-ratio effects in woven composite DCB specimens for a multi-directional layup. Int J Fatigue 2017;96:237–51. https://doi.org/10.1016/j.ijfatigue.2016.12.005.

[5] Liu Y, Zhang C. A critical plane-based model for mixed-mode delamination growth rate prediction under fatigue cyclic loadings. Compos B Eng 2018;139:185–94. https://doi.org/10.1016/j.compositesb.2017.11.053.

[6] Jones R, Kinloch AJ, Michopoulos JG, Brunner AJ, Phan N. Delamination growth in polymer-matrix fibre composites and the use of fracture mechanics data for material characterisation and life prediction. Compos Struct 2017;180:316–33. https://doi.org/10.1016/j.compstruct.2017.07.097.

[7] Jones R, Kinloch AJ, Hu W. Cyclic-fatigue crack growth in composite and adhesively-bonded structures: the FAA slow crack growth approach to certification and the problem of similitude. Int J Fatigue 2016;88:10–8. https://doi.org/10.1016/j.ijfatigue.2016.03.008.

[8] Ratwani MM, Kan HP. Compression fatigue analysis of fiber composites. J Aircr 1981;18:458–62. https://doi.org/10.2514/3.57512.

[9] A, Poursartip, N, Chinatambi, Fatigue Damage Development in Notched (0. Compos. Mater. Fatigue Fract. Second Vol., 100 Barr Harbor Drive, PO Box C700, West Conshohocken, PA 19428-2959: ASTM International; 2008, p. 45-45–21. 10.1520/STP10408S.

[10] Hojo M, Tanaka K, Gustafson CG, Hayashi R. Effect of stress ratio on near-threshold propagation of delimination fatigue cracks in unidirectional CFRP. Compos Sci Technol 1987;29:273–92. https://doi.org/10.1016/266-3538(87)90076-5.

[11] Masaki H, Shojiro O, Gustafson C-G, Keisuke T. Effect of matrix resin on delamination fatigue crack growth in CFRP laminates. Eng Fract Mech 1994;49: 35–47. https://doi.org/10.1016/013-7944(94)90109-0.

[12] Jones R, Pitt S, Bunner AJ, Hui D. Application of the Hartman-Schijve equation to represent Mode I and Mode II fatigue delamination growth in composites. Compos Struct 2012;94:1343–51. https://doi.org/10.1016/j.compstruct.2011.11.030.

[13] Andersons J, Hojo M, Ochiai S. Empirical model for stress ratio effect on fatigue delamination growth rate in composite laminates. Int J Fatigue 2004;26:597–604. https://doi.org/10.1016/j.ijfatigue.2003.10.016.

[14] Atodaria DR, Putatunda SK, Mallick PK. A fatigue crack growth model for random fiber composites. J Compos Mater 1997;31:1838–55. https://doi.org/10.1177/002199839703101804.

[15] Atodaria DR, Putatunda SK, Mallick PK. Fatigue crack growth model and mechanism of a random fiber SMC composite. Polym Compos 1999;20:240–9. https://doi.org/10.1002/pc.10351.

[16] G, Roderick, R, Everett, J, Crews Debond Propagation in Composite-Reinforced Metals. Fatigue Compos. Mater., 100 Barr Harbor Drive, PO Box C700, West Conshohocken, PA 19428-2959: ASTM International; 1974, p. 295-295–12. 10.1520/STP33179S.

[17] S, Mostovoy, EJ, Ripling Flaw Tolerance of a Number of Commercial and Experimental Adhesives. Adhes. Sci. Technol., Boston, MA: Springer US; 1975, p. 513–62. 10.1007/978-1-4613-4331-8_9.

[18] R, Martin, G, Murri Characterization of Mode I and Mode II delamination Growth and Thresholds in AS4/PEEK Composites. Compos Mater Test Des (Ninth Vol 2009: 251-251–20. 10.1520/stp24115s.

[19] Andersons J, Hojo M, Ochiai S. Model of delamination propagation in brittle-matrix composites under cyclic loading. J Reinf Plast Compos 2001;20:431–50. https://doi.org/10.1106/JGY1-GH43-ET2U-C193.

[20] Brussat TR, Chiu ST. Fatigue crack growth of bondline cracks in structural bonded joints. J Eng Mater Technol 1978;100:39–45. https://doi.org/10.1115/1.3443448.

[21] R, Ramkumar, J, Whitcomb Characterization of Mode I and Mixed-Mode Delamination Growth in T300/5208 Graphite/Epoxy. Delamination Debonding Mater., 100 Barr Harbor Drive, PO Box C700, West Conshohocken, PA 19428-2959: ASTM International; 1985, p. 315-315–21. 10.1520/STP36312S.

[22] Kenane M, Benzeggagh ML. Mixed-mode delamination fracture toughness of unidirectional glass/epoxy composites under fatigue loading. Compos Sci Technol 1997;57:597–605. https://doi.org/10.1016/S0266-3538(97)00021-3.

[23] Shivakumar K, Chen H, Abali F, Le D, Davis C. A total fatigue life model for mode I delaminated composite laminates. Int J Fatigue 2006;28:33–42. https://doi.org/10.1016/j.ijfatigue.2005.04.006.

[24] Alderliesten RC, Brunner AJ, Pascoe JA. Cyclic fatigue fracture of composites: what has testing revealed about the physics of the processes so far? Eng Fract Mech 2018;203:186–96. https://doi.org/10.1016/j.engfracmech.2018.06.023.

[25] Gong Y, Zhao L, Zhang J, Hu N, Zhang C. An insight into three approaches for determining fatigue delamination resistance in DCB tests on composite laminates. Compos Part B Eng 2019;176:107206. https://doi.org/10.1016/j.compositesb.2019.107206.

[26] Pascoe JA, Alderliesten RC, Benedictus R. Methods for the prediction of fatigue delamination growth in composites and adhesive bonds – a critical review. Eng Fract Mech 2013;112–113:72–96. https://doi.org/10.1016/j.engfracmech.2013.10.003.

[27] Gong Y, Zhao L, Zhang J, Hu N. A novel model for determining the fatigue delamination resistance in composite laminates from a viewpoint of energy. Compos Sci Technol 2018;167:489–96. https://doi.org/10.1016/j.compscitech.2018.08.045.

[28] Pascoe JA, Alderliesten RC, Benedictus R. On the physical interpretation of the R-ratio effect and the LEFM parameters used for fatigue crack growth in adhesive bonds. Int J Fatigue 2017;97:162–76. https://doi.org/10.1016/j.ijfatigue.2016.12.033.

[29] Yao L, Alderliesten RC, Benedictus R. The effect of fibre bridging on the Paris relation for mode I fatigue delamination growth in composites. Compos Struct 2016;140:125–35. https://doi.org/10.1016/j.compstruct.2015.12.027.

[30] Trabal GG, Bak BLV, Chen B, Jensen SM, Lindgaard E. Delamination toughening of composite laminates using weakening or toughening interlaminar patches to initiate multiple delaminations: a numerical study. Eng Fract Mech 2022;273: 108730. https://doi.org/10.1016/j.engfracmech.2022.108730.

[31] Gong Y, Li W, Liu H, Yuan S, Wu Z, Zhang C. A novel understanding of the normalized fatigue delamination model for composite multidirectional laminates. Compos Struct 2019;229:111395. https://doi.org/10.1016/j.compstruct.2019.111395.

[32] Pascoe JA, Zarouchas DS, Alderliesten RC, Benedictus R. Using acoustic emission to understand fatigue crack growth within a single load cycle. Eng Fract Mech 2018; 194:281–300. https://doi.org/10.1016/j.engfracmech.2018.03.012.

[33] Alderliesten RC. How proper similitude can improve our understanding of crack closure and plasticity in fatigue. Int J Fatigue 2016;82:263–73. https://doi.org/10.1016/j.ijfatigue.2015.04.011.

[34] Rans C, Alderliesten R, Benedictus R. Misinterpreting the results: How similitude can improve our understanding of fatigue delamination growth. Compos Sci Technol 2011;71:230–8. https://doi.org/10.1016/j.compscitech.2010.11.010.

[35] Griffith AVI. The phenomena of rupture and flow in solids. Philos Trans R Soc London Ser A, Contain Pap a Math or Phys Character 1921;221:163–98. https://doi.org/10.1098/rsta.1921.0006.

[36] Pascoe JA, Alderliesten RC, Benedictus R. On the relationship between disbond growth and the release of strain energy. Eng Fract Mech 2015;133:1–13. https://doi.org/10.1016/j.engfracmech.2014.10.027.

[37] Amaral L, Yao L, Alderliesten R, Benedictus R. The relation between the strain energy release in fatigue and quasi-static crack growth. Eng Fract Mech 2015;145: 86–97. https://doi.org/10.1016/j.engfracmech.2015.07.018.

[38] Pascoe JA, Alderliesten RC, Benedictus R. Towards understanding fatigue disbond growth via cyclic strain energy. Procedia Mater Sci 2014;3:610–5. https://doi.org/10.1016/j.mspro.2014.06.101.

[39] Yao L, Alderliesten RC, Zhao M, Benedictus R. Discussion on the use of the strain energy release rate for fatigue delamination characterization. Compos Part A Appl Sci Manuf 2014;66:65–72. https://doi.org/10.1016/j.compositesa.2014.06.018.

[40] Yao L, Sun Y, Guo L, Lyu X, Zhao M, Jia L, et al. Mode I fatigue delamination growth with fibre bridging in multidirectional composite laminates. Eng Fract Mech 2018;189:221–31. https://doi.org/10.1016/j.engfracmech.2017.11.013.

[41] Brunner AJ, Stelzer S, Pinter G, Terrasi GP. Cyclic fatigue delamination of carbon fiber-reinforced polymer-matrix composites: data analysis and design considerations. Int J Fatigue 2016;83:293–9. https://doi.org/10.1016/j.ijfatigue.2015.10.025.

[42] Ferreira Motta Jr R, Alderliesten R, Yutaka Shiino M, Odila Hilário Cioffi M, Jacobus Cornelis Voorwald H. Scrutinizing interlaminar fatigue loading cycle in composites using acoustic emission technique: stress ratio influence on damage formation. Compos Part A Appl Sci Manuf 2020;138:106065. https://doi.org/10.1016/j.compositesa.2020.106065.

[43] YA, Dzenis Cycle-based analysis of damage and failure in advanced composites under fatigue: 1. Experimental observation of damage development within loading cycles. Int J Fatigue 2003;25:499–510. 10.1016/jS0142-1123(02)00170-6.

[44] Xiang Y, Liu R, Peng T, Liu Y. A novel subcycle composite delamination growth model under fatigue cyclic loadings. Compos Struct 2014;108:31–40. https://doi.org/10.1016/j.compstruct.2013.09.003.

[45] Al-Jumaili SK, Eaton MJ, Holford KM, Pearson MR, Crivelli D, Pullin R. Characterisation of fatigue damage in composites using an acoustic emission parameter correction technique. Compos Part B Eng 2018;151:237–44. https://doi.org/10.1016/j.compositesb.2018.06.020.

[46] Bohmann T, Schlamp M, Ehrlich I. Acoustic emission of material damages in glass fibre-reinforced plastics. Compos Part B Eng 2018;155:444–51. https://doi.org/10.1016/j.compositesb.2018.09.018.

[47] Gutkin R, Green CJ, Vangrattanachai S, Pinho ST, Robinson P, Curtis PT. On acoustic emission for failure investigation in CFRP: pattern recognition and peak frequency analyses. Mech Syst Signal Process 2011;25:1393–407. https://doi.org/10.1016/j.ymssp.2010.11.014.

[48] Barile C, Casavola C, Pappalettera G, Vimalathithan PK. Damage characterization in composite materials using acoustic emission signal-based and parameter-based data. Compos Part B Eng 2019;178:107469. https://doi.org/10.1016/j.compositesb.2019.107469.

[49] M, Sause, M, Hamstad 7.14 Acoustic Emission Analysis. Compr. Compos. Mater. II, vol. 7, Elsevier; 2018, p. 291–326. Doi: B978-0-12-803581-8.10036-0.

[50] Kempf M, Skrabala O, Altstädt V. Acoustic emission analysis for characterisation of damage mechanisms in fibre reinforced thermosetting polyurethane and epoxy. Compos Part B Eng 2014;65:117–23. https://doi.org/10.1016/j.compositesb.2014.05.003.

[51] Oz FE, Ersoy N, Lomov SV. Do high frequency acoustic emission events always represent fibre failure in CFRP laminates? Compos Part A Appl Sci Manuf 2017; 103:230–5. https://doi.org/10.1016/j.compositesa.2017.10.013.

[52] Crivelli D, Guagliano M, Eaton M, Pearson M, Al-Jumaili S, Holford K, et al. Localisation and identification of fatigue matrix cracking and delamination in a carbon fibre panel by acoustic emission. Compos Part B Eng 2015;74:1–12. https://doi.org/10.1016/j.compositesb.2014.12.032.

[53] Ben Ameur M, El Mahi A, Rebiere J-L, Gimenez I, Beyaoui M, Abdennadher M, et al. Investigation and identification of damage mechanisms of unidirectional carbon/flax hybrid composites using acoustic emission. Eng Fract Mech 2019;216:106511. https://doi.org/10.1016/j.engfracmech.2019.106511.

[54] Maillet E, Baker C, Morscher GN, Pujar VV, Lemanski JR. Feasibility and limitations of damage identification in composite materials using acoustic emission. Compos Part A Appl Sci Manuf 2015;75:77–83. https://doi.org/10.1016/j.compositesa.2015.05.003.

[55] Chen H, Shivakumar KN, Abali F. Application of total fatigue life model to T700 carbon/vinyl ester composite. Compos Part B Eng 2008;39:36–41. https://doi.org/10.1016/j.compositesb.2007.02.019.

[56] D5528-13.. Standard test method for mode I interlaminar fracture toughness of unidirectional fiber-reinforced polymer matrix composites. ASTM B Stand 2013;01:1–12. https://doi.org/10.1520/D5528-01R07E03.2.

[57] G, Technique, Composites T. D3171-15 Standard Test Methods for Constituent Content of Composite Materials 2000;76:1–10. 10.1520/D3171-15.2.

[58] R, Alderliesten, AJ, Brunner Determination of Mode I Fatigue Delamination Propagation in Unidirectional Fibre-Reinforced Polymer Composites - ESIS TC 4 Test Protocol 2019;1:1–14.

[59] ASTM-E976-15.. Standard guide for determining the reproducibility of acoustic emission sensor response. Am Soc Test Mater 2015.

[60] Bourchak M, Farrow I, Bond I, Rowland C, Menan F. Acoustic emission energy as a fatigue damage parameter for CFRP composites. Int J Fatigue 2007;29:457–70. https://doi.org/10.1016/j.ijfatigue.2006.05.009.

[61] Saeedifar M, Zarouchas D. Damage characterization of laminated composites using acoustic emission: a review. Compos Part B Eng 2020;195:108039. https://doi.org/10.1016/j.compositesb.2020.108039.

[62] Pascoe JA, Alderliesten RC, Benedictus R. Characterising resistance to fatigue crack growth in adhesive bonds by measuring release of strain energy. Procedia Struct Integr 2016;2:80–7. https://doi.org/10.1016/j.prostr.2016.06.011.

[63] Shiino MY, Pelosi TS, Cioffi MOH, Donadon MV. The Role of stitch yarn on the delamination resistance in non-crimp fabric: chemical and physical interpretation. J Mater Eng Perform 2017;26:978–86. https://doi.org/10.1007/s11665-016-2460-2.

[64] Dathe A, Tarquis AM, Perrier E. Multifractal analysis of the pore- and solid-phases in binary two-dimensional images of natural porous structures. Geoderma 2006;134:318–26. https://doi.org/10.1016/j.geoderma.2006.03.024.

[65] AJ, Brunner, Correlation between acoustic emission signals and delaminations in carbon fiber-reinforced polymer-matrix composites: a new look at mode I fracture test data. 32nd Eur Conf Acoust Emiss 2016:55–64.

[66] Maugis D. Subcritical crack growth, surface energy, fracture toughness, stick-slip and embrittlement. J Mater Sci 1985;20:3041–73. https://doi.org/10.1007/BF00545170.

[67] Saeedifar M, Fotouhi M, Ahmadi Najafabadi M, Hosseini Toudeshky H, Minak G. Prediction of quasi-static delamination onset and growth in laminated composites by acoustic emission. Compos Part B Eng 2016;85:113–22. https://doi.org/10.1016/j.compositesb.2015.09.037.

[68] Arumugam V, Saravanakumar K, Santulli C. Damage characterization of stiffened glass-epoxy laminates under tensile loading with acoustic emission monitoring. Compos Part B Eng 2018;147:22–32. https://doi.org/10.1016/j.compositesb.2018.04.031.

[69] Kotsikos G, Evans JT, Gibson AG, Hale J. Use of acoustic emission to characterize corrosion fatigue damage accumulation in glass fiber reinforced polyester laminates. Polym Compos 1999;20:689–96. https://doi.org/10.1002/pc.10392.

[70] Lissek F, Haeger A, Knoblauch V, Hloch S, Pude F, Kaufeld M. Acoustic emission for interlaminar toughness testing of CFRP: evaluation of the crack growth due to burst analysis. Compos Part B Eng 2018;136:55–62. https://doi.org/10.1016/j.compositesb.2017.10.012.

[71] Bak BLV, Sarrado C, Turon A, Costa J. Delamination under fatigue loads in composite laminates: a review on the observed phenomenology and computational methods. Appl Mech Rev 2014;66. https://doi.org/10.1115/1.4027647.

[72] Yao L, Sun Y, Guo L, Alderliesten RC, Benedictus R, Zhao M, et al. Fibre bridging effect on the Paris relation of mode I fatigue delamination in composite laminates with different thicknesses. Int J Fatigue 2017;103:196–206. https://doi.org/10.1016/j.ijfatigue.2017.06.004.

[73] Alderliesten R. Fatigue delamination of composite materials – approach to exclude large scale fibre bridging. IOP Conf Ser Mater Sci Eng 2018;388:012002. https://doi.org/10.1088/1757-899X/388/1/012002.

[74] GB, Murri Evaluation of delamination onset and growth characterization methods under mode i fatigue loading. 27th Annu Tech Conf Am Soc Compos 2012, Held Jointly with 15th Jt US-Japan Conf Compos Mater ASTM-D30 Meet 2012:601–20.